

Linköping University | Department of Electrical Engineering

Master's thesis, 30 ECTS | Applied Physics

2023 | LIU-ISY/LITH-EX-A--23/5621--SE

Development of a QRNG front-end for shot noise measurement

- analysis of quantum shot noise originating from photodiodes

Utveckling och analys av förstärkt skottbrus från fotodioder för applikation inom kvantslumptalsgenerering

Martin Clason

Supervisor : Joakim Argillander
Examiner : Guilherme B. Xavier

Upphovsrätt

Detta dokument hålls tillgängligt på Internet - eller dess framtida ersättare - under 25 år från publiceringsdatum under förutsättning att inga extraordinära omständigheter uppstår.

Tillgång till dokumentet innebär tillstånd för var och en att läsa, ladda ner, skriva ut enstaka kopior för enskilt bruk och att använda det oförändrat för ickekommersiell forskning och för undervisning. Överföring av upphovsrätten vid en senare tidpunkt kan inte upphäva detta tillstånd. All annan användning av dokumentet kräver upphovsmannens medgivande. För att garantera äktheten, säkerheten och tillgängligheten finns lösningar av teknisk och administrativ art.

Uphovsmannens ideella rätt innehåller rätt att bli nämnd som upphovsman i den omfattning som god sed kräver vid användning av dokumentet på ovan beskrivna sätt samt skydd mot att dokumentet ändras eller presenteras i sådan form eller i sådant sammanhang som är kränkande för upphovsmannens litterära eller konstnärliga anseende eller egenart.

För ytterligare information om Linköping University Electronic Press se förlagets hemsida <http://www.ep.liu.se/>.

Copyright

The publishers will keep this document online on the Internet - or its possible replacement - for a period of 25 years starting from the date of publication barring exceptional circumstances.

The online availability of the document implies permanent permission for anyone to read, to download, or to print out single copies for his/hers own use and to use it unchanged for non-commercial research and educational purpose. Subsequent transfers of copyright cannot revoke this permission. All other uses of the document are conditional upon the consent of the copyright owner. The publisher has taken technical and administrative measures to assure authenticity, security and accessibility.

According to intellectual property law the author has the right to be mentioned when his/her work is accessed as described above and to be protected against infringement.

For additional information about the Linköping University Electronic Press and its procedures for publication and for assurance of document integrity, please refer to its www home page: <http://www.ep.liu.se/>.

Abstract

As one of the more mature quantum technologies, quantum random number generators (QRNGs) fill an important role in producing secure and private keys for use in cryptography in e.g. quantum key distribution (QKD) systems. Many available QRNGs are expensive and optical QRNGs often require complex optical setups. If a reliable QRNG could be implemented using less expensive components they could become more widespread and be used in common applications like encryption and simulation. Shot noise is a possible entropy source for these kinds of random number generators. For such a generator to be classified as a QRNG the origin of the shot noise must be controlled and verifiable. This project aims to investigate how an entropy source could be implemented using the shot noise generated by an illuminated photodiode. This requires the design and construction of the accompanying electro-optical front-end used to prepare a signal for sampling.

The successful estimation of the electron charge e is used as a way to verify that shot noise is present in the sampled signal. Suitable component values and operating points are also investigated and it is shown that quite low gain (10 000) is suitable for the current-to-voltage amplifier which amplifies the signal generated by the photodiode. For this configuration an estimate of e was achieved with a relative error of 3%.

In conclusion this is a promising and interesting approach for generating random numbers at high rates and at low cost. Whether the correct estimation of e is enough to certify that the device is sampling noise from the quantum regime is however not completely clear and further investigation is likely needed.

Acknowledgments

First off, I would like to thank Joakim and Guilherme for answering "Of course we have something for you!" when I, somewhat stressed about not finding a thesis, reached out to them about writing my master thesis with them.

I'm so grateful for my partner Antonia who helped and put up with me, especially during the last weeks of the project. I would not be able to be finished by now without your help! A big thank you to my friend Erik Böhlén for bringing some components and material that I needed shipped across the country and for stopping by the lab, cheering me on when I was knees deep in troubleshooting paradise. Thank you to Titus Wuermeling, my new friend from Germany, who studied with me and kept me company during report writing. I also want to thank my father for his interest in the progress of the project and for bouncing ideas regarding the electronics, but also that he lent me the photodiode amplifier book [1], which was almost critical for this project I think. It's crazy that this book has been in the bookshelf at home all my life and I realized it existed just now...

I'm really grateful to have Professor Guilherme B. Xavier as my examiner. You have really shown interest in this and often stopped by the lab to chat with me and check on the progress of the project. I don't think this would be the case for every examiner out there, so thank you! I also want to thank all the other co-workers and students at the department for chatting with me and showing interest in the project. I would especially like to thank Robert Forchheimer for valuable input and taking your time to help Joakim and me when we tried to understand some peculiar behaviour of a simulation.

Last but not least, thank you again to my supervisor Joakim for always helping out and discussing issues or ideas. You have really invested a lot in me and this project! I'm delighted to be able to continue this collaboration in future research!

It has been really nice to write my thesis at the quantum technologies laboratory, so thank you all!

(Also thank you to Analog Devices for supplying free samples of some really good amplifiers. I might've fried a couple though...)

Martin Clason
Linköping, November 2023

Contents

Abstract	iii
Acknowledgments	iv
Contents	v
Abbreviations	vii
List of Figures	ix
List of Tables	xi
1 Introduction	1
1.1 Motivation	1
1.1.1 Previous work	2
1.2 Aim	2
1.3 Research questions	3
1.4 Delimitations	3
2 Theory	4
2.1 Random number generators	4
2.1.1 Pseudorandom number generators (PRNG) vs true random number generators (TRNG)	4
2.1.2 Quantum random number generators (QRNG)	5
2.2 Photon statistics	6
2.2.1 Quantum theory of photodetection	7
2.2.2 Effect of losses on photon statistics	7
2.2.3 Electrons vs photons	7
2.2.4 LEDs vs lasers as light sources	8
2.3 Noise	8
2.3.1 Noise sources in photodiodes	8
2.3.2 Shot noise	8
2.3.3 Thermal noise (Johnson-Nyquist noise)	9
2.3.4 $1/f$ noise (flicker noise)	10
2.3.5 Popcorn noise	10
2.3.6 Avalanche noise	10
2.4 Photodetection	10
2.4.1 Detector capacitance	11
2.4.2 Reverse bias	12
2.4.3 The LED as a light source	12
2.5 Design of the photodiode amplifier	13
2.5.1 Noise analysis of photodiode amplifier	15
2.5.2 Choice of operational amplifier for the TIA circuit	17

2.5.3	Stability and bandwidth	18
2.6	Signal to noise ratio for shot noise and thermal noise	19
3	Method	20
3.1	Design	20
3.1.1	Optical front-end	20
3.1.2	Electrical front-end	20
3.2	Implementation	21
3.2.1	Measurement box	21
3.2.2	Prototype circuit board	22
3.2.3	Choice of component values & filter parameters	22
3.3	Evaluation	24
3.3.1	Noise floor	24
3.3.2	Transfer function of the amplifier	24
3.3.3	Shot noise measurements	24
3.3.4	Estimation of electron charge	24
4	Results & Discussion	26
4.1	Noise floor of the complete system	26
4.2	Transfer function of the amplifier	28
4.3	Evaluation of the shot noise front-end	29
4.3.1	Photodiode response to LED illumination	29
4.3.2	Evaluation of RMS fluctuations in noise as function of drive current	30
4.3.3	Frequency spectrum analysis of noise	31
4.3.4	Estimation of electron charge	35
4.4	General discussion	41
4.4.1	Discussion of method	42
4.5	The work in a wider context	42
5	Conclusion	44
5.1	Future work	44
Bibliography		45
A Images		46

Abbreviations

AC Alternating current

ADC Analog to digital converter

APD Avalanche photodiode

CCD Charge-coupled device

CMOS

Complementary metal-oxide semiconductor

DC Direct current

DSO Digital storage oscilloscope. An oscilloscope with the capability to capture and store waveforms or samples on a digital medium like a USB drive.

DUT Device under test, in this case often the prototype board characterized in the experiments.

EHP Electron hole pair

FET Field effect transistor

FFT Fast fourier transform

IC Integrated circuit

LED Light emitting diode

NEP Noise equivalent power

op amp, opa

Operational amplifier

PCB Printed circuit board

PD Photodiode

PIN diode

A type of diode that has a wide layer of intrinsic semiconductor material between the p-type and n-type doped regions.

PRNG

Pseudorandom number generator

PSD Power spectral distribution

QRNG

Quantum random number generator

RMS Root mean square

RNG Random number generator

SMT, SMD

Surface-mount technology or surface mount device refers to electrical components that are mounted onto soldering pads on the surface of PCBs. This is in contrast with classical components with leads that are mounted in holes on the circuit board.

SNR Signal to noise ratio

TIA, Tz amp

Transimpedance amplifier

TRNG

True random number generator

List of Figures

2.1	Example setup for a branching path random number generator utilizing a source that emits photons, a beam splitter and two detectors (D1 and D2) detecting the photons.	6
2.2	Approximate photodiode model with parasitic elements.	11
2.3	Illustration of how the PN-junction relates to the diode and where the depletion region is located. The electrical field resulting from the reverse bias and the built in field E_0 are also shown. The solid line in the middle is where the two differently doped semiconductors are joined, sometimes called the metallurgical junction. The regions outside the depletion region are referred to as neutral regions.	12
2.4	Alternative circuits for monitoring signal from photodiode.	14
2.5	Noise model of photodiode amplifier with noise sources and parasitic elements.	15
2.6	Noise spectral distribution of the noise voltage at the circuits output [1]	17
3.1	The schematic of the complete front-end including photodiode bias and power supply circuitry.	21
3.2	The complete prototype circuit board with amplifier and an LED in blue directed towards the transparent photodiode.	22
4.1	The noise floor of the system at different configurations.	27
4.2	The transfer function of the amplifier between 10 Hz and 25 MHz for four different amplifications across the tested range. The magnitude is normalized to their respective expected amplifications.	28
4.3	The response of the photodiode amplifier for different drive currents and different resistor values where $\langle V_{\text{out}} \rangle$ denotes the time-average of the amplifier output.	29
4.4	The response of the photodiode amplifier for different drive currents normalized using the respective amplifications (i.e. the same but rescaled data as in fig. 4.3).	30
4.5	The RMS of the obtained noise plotted against the applied LED driving current for all amplifications.	30
4.6	RMS of the V_{out} noise plotted against the resulting mean photocurrent i_{pc}	31
4.7	Spectrum using FFT for AC-coupled data for all gains at zero drive current of the LED (but with the sourcemeter turned on and connected to the system).	32
4.8	Spectrum using FFT for AC-coupled data for all amplifications at an LED drive current of 100 μA	33
4.9	Fourier spectrum for AC-coupled data for all amplifications at an LED drive current of 1 mA. (There is no data for the highest amplification at 1 mA caused by saturation of the amplifier.)	34
4.10	Rescaled squared RMS of V_{out} plotted against the resulting mean photocurrent i_{pc} . The slope should equal the electron charge, e , which is plotted in grey line with dashes and dots. The regression line used to obtain the estimate q is inside the shaded area and plotted in black with a dashed line.	36

4.11	Rescaled squared RMS of V_{out} plotted against the resulting mean photocurrent i_{pc} . The slope should equal the electron charge, e , which is plotted in grey line with dashes and dots. The regression line used to obtain the estimate q is inside the shaded area and plotted in black with a dashed line.	38
4.12	Rescaled squared RMS of V_{out} plotted against the resulting mean photocurrent i_{pc} . The slope should equal the electron charge, e , which is plotted in grey line with dashes and dots. The regression line used to obtain the estimate q is inside the shaded area and plotted in black with a dashed line.	40
A.1	The measurement box that was constructed during the project. SMA connectors can be seen on the front side to allow pass-through of cables for driving or measuring signals.	46
A.2	The prototype equipped with batteries inside the shielding box ready for performing measurements.	47
A.3	The operational amplifier mounted on the prototype board "dead bug"-style (i.e. upside down).	47

List of Tables

3.1	Frequency ranges corresponding to the lowest voltage noise contribution for the different amplifications R_f and the upper cutoff of the bandwidth (given by f_{pf}).	23
3.2	Si PIN photodiode TEFD4300 specifications [11]	23
3.3	Tested values of R_f	25
3.4	Applied driving currents I_{dr} of the LED during measurement runs.	25
4.1	Resulting estimates of e when using raw data and the whole bandwidth of the sample data.	37
4.2	Resulting estimates of e when using optimally filtered data and the corresponding bandwidths.	39
4.3	Resulting estimates of e when using arbitrarily filtered data and the corresponding bandwidth. The same pass-band of 8 MHz to 15 MHz was used for all measurements.	41

Introduction

In this chapter the motivation for using and developing quantum random number generators (QRNGs) is presented. The purpose and delimitations of the project are also stated.

1.1 Motivation

Secure communication is a fundamental need in any society and if quantum key distribution systems are implemented it can become even more secure and reliable with better guarantees. A QKD system could be utilized to distribute cryptographic keys between parties which then can use the key to encrypt and transmit data using encryption schemes like one-time-pad (which is uncrackable if the key is assumed to be private). Even if the distribution system was considered completely secure the overall security would depend completely on the security and privacy of the keys that are distributed. Secure communication in society therefore hinges on the secure and private generation of random numbers at high speed and on demand. A system which solely relies on the security of the key works in accordance with Kerckhoffs's principle [2] and one possible technology to use for key generation are QRNGs.

Generation of random numbers is not only important in cryptography but also in many other applications. Random numbers can be used to generate interesting worlds and landscapes in games, to run Monte-Carlo simulations [2] for e.g. research in material physics etc. These applications only require random numbers that are evenly distributed and that there are no particular patterns in the data. Generating cryptographic keys requires, however, not only that the generated data is evenly distributed, but also that it is private. This means that the generated sequence of random numbers should only be known to the user and not an eavesdropping attacker. The notion of randomness and the requirement of no patterns in the data can also be described using the following thought experiment. If an attacker had unlimited computing power and access to a stream of random bits from a random number generator, they should have no more than 50% chance of guessing the subsequent bit correctly, even if they have access to the whole history of generated bits before this next bit.

A common type of RNG is a generator implemented in code using a seed (a starting value). These are referred to as pseudorandom number generators (PRNGs) since their output sequence is in essence determined completely by their starting seed. This follows from computer programs being fully deterministic and therefore if you know the initial state, you know all subsequent states and thus also what numbers it will generate. This in turn means that an attacker, given a sufficiently long stream of generated data, could be able to determine the internal state of this generator and in turn also correctly predict future generated bits. This is

not a particularly desirable property when using your generator to construct cryptographic keys that should be private.

Computer programs on their own are not sufficient when generating secure keys. A different approach could be to sample a physical system in order to generate random bits from the state of the system. Many chaotic systems appear random in nature while they really are fundamentally deterministic. These chaotic physical systems are of course very complex but nonetheless still deterministic since its evolution always depends on the previous state of the system. A concrete example of this, which actually has been implemented [3], is to construct a random generator using the seemingly random behaviour of bubbles in lava lamps. If this system is used to generate cryptographic keys a very powerful attacker, with knowledge of how this generator works, would probably be able to analyse your generated random numbers and build up a model of the current state of your lava lamp. With this model she could be able to predict how the next bubble should form and thus be able to predict what numbers the generator will generate next. This can often be the case for true random number generators based on classical systems.

Hence you cannot use most physical systems since they are inherently deterministic, so where should you turn in order to find an intrinsically stochastic physical system? Of course you turn to the world of quantum physics! According to our current understanding, quantum mechanics is the only theory that offers true randomness [2].

Existing optical QRNGs can use many different phenomena like time of arrival statistics for photons, path superposition of single photons using two detectors, photon counting statistics using photon counting detectors or homodyne detection of shot noise originating from vacuum fluctuations using a laser [2]. Many of these require quite complex and expensive components and can also consume a lot of space [4].

1.1.1 Previous work

There are also less complex setups which try to optically generate random numbers of quantum origin. One setup uses CCD or CMOS cameras to measure shot noise and generate random numbers [4]. The number of photons detected in each pixel is used as the entropy source and then randomness extraction (explained in section 2.1) is performed to retrieve the final bit string. To show in which region quantum shot noise dominates they calculate the Fano factor (the ratio of variance and mean) which should be 1 for Poissonian statistics.

Another generator measures shot noise from a photodiode illuminated by a LED. It samples a free running clock when the noise amplitude crosses a threshold which is determined from measurements of the background noise when the illuminating LED is switched off [5].

1.2 Aim

The aim of this project is to investigate shot noise in LEDs and photodiodes. The purpose of this is to explore the possibility of constructing a low-cost quantum random number generator. The focus is on understanding the quantum nature of these devices and if it is possible to certify or prove that it is a quantum process you are collecting entropy from. It is interesting to look into this as existing QRNGs usually are quite complex and require more expensive components whereas a QRNG based on the setup investigated in this project has the potential to be simpler and of lower cost. It must still however be able to supply a good source of entropy for random number generation and still preferably be considered a QRNG. This project consists of the development, construction and evaluation of a potential analog front

end for a random number generator amplifying the noise signal coming from an illuminated photodiode.

1.3 Research questions

The aim of this thesis project is to try to answer the following questions:

1. How can a front-end for measuring shot noise originating from a photodiode be constructed?
2. What are some important considerations to take into account when constructing a QRNG using this scheme?
3. Is it possible to certify or determine whether the system is sampling noise with true quantum origin?

1.4 Delimitations

This work is limited to investigating the shot noise behaviour of LED-to-photodiode couplers and potential avenues of approach for generating random numbers using this noise. The scheme of digitization of the noise signal from the entropy source is not investigated and random numbers are thus not generated in this work. Extraction is thus also not included in this project.

The speed and bandwidth of the front end will limit the final generation bit rate of a prospective random number generator building on this front-end. Thus high bandwidth is one of the more important aspects of the front-end. The DSO that is used to acquire samples during measurements in this project is however limited to 2.5 GSa/s and the Bode plot functionality of this oscilloscope is limited to 25 MHz. The analysis in this project is thus limited to only cover frequencies up to 25 MHz. The components should however be chosen to allow for higher bitrates than this. Since high generation bit rate is a very important metric for most applications, a potential expansion on this project would probably utilize a discrete ADC chip to achieve higher sample rates than what is analysed in this work.

Theory

In the worst-case scenario for a classical system, it could be assumed that an adversary has control over or access to other noise sources in the system. These include technical noise from the circuit components and, for instance, thermal noise generated in the feedback resistance (R_f in fig. 3.1) that controls the gain of the amplifier. Somehow, the system has to be able to extract private randomness originating from a quantum entropy source, in this project, shot noise from the arrival of photons. It also has to be certified or proven that this is the case for the random number generator in order to be able to refer to it as a quantum random number generator (QRNG).

For classical generators there are examples of attacks both on algorithms used for random number generation as well as attacks on the hardware itself (e.g. by changing the dopant levels in some electrical components) to introduce back doors that may be used by an attacker to retrieve generated numbers [2].

2.1 Random number generators

This section briefly covers different types of random number generators and their characteristics.

2.1.1 Pseudorandom number generators (PRNG) vs true random number generators (TRNG)

If numbers that only mimic "true randomness" are needed PRNGs can be used since they in actuality are completely deterministic. Another way to look at it is that the only entropy present from the output of a PRNG is the entropy that was available in the starting seed and thus the entropy is constant for PRNGs [2]. This seed can in turn be taken from another source which could be more random. An interesting result following from these kinds of generators really being state machines, is that their generated sequence has to repeat itself since the generator is constructed with finite memory, which of course always is the case for real computers. Because of this an important measure is their periodicity, i.e. how often they will start to repeat their output and this period should of course be as long as possible for most applications.

The main advantages of PRNGs is that they can be quite fast and also maybe unintuitively that they are deterministic. The deterministic nature means that for applications like simulations it is perfectly possible to generate the exact same simulation results again as long as you

start with the same seed, even though vast amounts of "random" data from the generator was needed for the simulation. In other words their generated sequences are reproducible [2].

These characteristics are in contrast with true random number generators which use some unpredictable (in some cases though just difficult to predict) physical processes. The sampling of these systems is often referred to as entropy gathering and sources like timing of interrupts from keyboard interactions, mouse movements or data from the sound card are common examples. Sometimes the distinction between these and physical TRNGs is made and the physical kind then refers to generators that sample systems with more profound physical effects like chaotic systems, thermal noise of electronic circuits or biometric parameters [2].

Since pseudorandom generators use a deterministic process you are limited to evaluating their product, i.e. the output strings, and subject them to various statistical tests in order to try to check if they are indistinguishable enough from randomness. When evaluating a TRNG that samples a process you can instead focus on checking or certifying that the process is behaving randomly. When checking this process for random behaviour though you have to be wary of the model you use. It might be the case that it seems to behave randomly for a given model but if a more complicated model were to be used it might suddenly appear to behave quite predictably. This can be the case for many classical systems and in this regard using quantum systems as the entropy source effectively eliminates this issue since the inherent random nature of these systems are often well-defined and doesn't really need to be modeled [2].

2.1.1.1 Block structure of TRNG

Usually a TRNG (actually any RNG) can be divided into different blocks consisting of:

- Entropy source
 - Sampling and digitization
- Postprocessing
 - Randomness extraction

In practice, sampling and digitization are inherently noisy processes which thus contaminate the actual random variable that is measured. The purpose of the second block is to distill the raw bit strings from the measurement and try to extract as much randomness as possible. If it is successful the output is a uniform random bit sequence without bias. Extraction is in essence a lossy compression process that tries to compress the data to its entropic limit [2].

Some postprocessing algorithms can be slow, especially if they are constructed to throw away as little as possible, and thus some trade-offs might arise here. For instance, you might have a low quality raw bit string but with high bit rate which in turn requires fast postprocessing that discards lots of bits versus having a higher quality bit stream of low bit rate that requires almost no postprocessing [2].

2.1.2 Quantum random number generators (QRNG)

By sampling a quantum phenomenon a QRNG is able to gather entropy and in turn generate random numbers. Because they sample physical systems they are a particular instance

of physical TRNGs. Since quantum systems to the best of our knowledge and theories behave completely stochastic this is a physical source of entropy that doesn't rely on limited knowledge of a system which can be the case for classical physical TRNG [2].

One of the most straightforward QRNG schemes is path superposition of a single photon using a 50/50 beam splitter. In this setup, shown in fig. 2.1, a single photon is sent through a balanced beam splitter with one detector at each output. As an example a 0 bit could be added to the generated bit string if the photon was reflected and detected in detector D1 but a 1 bit could instead be generated if the photon was transmitted and detected in detector D2. The drawbacks of these systems are that the beam splitter needs to be perfectly balanced and unbiased but also that the detectors need to have equal detection efficiencies in order to guarantee equal detection probabilities for each path. The detection also requires single photon detectors which have an intrinsic dead time that limits the achievable bitrate of the generator. In practice this means generation rates on the order of Mb/s [2].

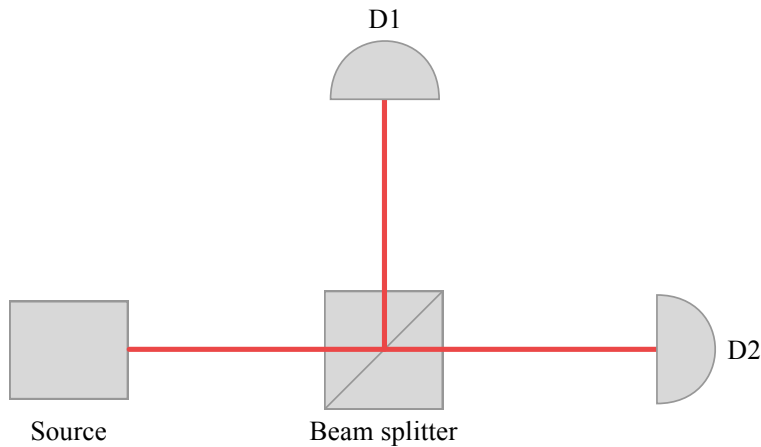


Figure 2.1: Example setup for a branching path random number generator utilizing a source that emits photons, a beam splitter and two detectors (D1 and D2) detecting the photons.

2.2 Photon statistics

For a perfectly coherent light source with constant power the average photon flux will obviously also be constant. For a given detection window however, the number of photons detected is not necessarily constant but will vary around this mean value of detections. The distribution of the number of photons in a given detection window is given by the Poissonian distribution in eq. (2.1) and this kind of light is therefore said to have Poissonian photon statistics.

$$P(n) = \frac{\bar{n}^n}{n!} e^{-\bar{n}}, \quad n = 0, 1, 2, \dots \quad (2.1)$$

where \bar{n} is the mean or the average photon flux. This randomness in essence comes from the fact that the energy has to be quantized into light quanta or photons [6].

Poisson distributions only have one parameter, the mean \bar{n} , since the variance $\sigma = \sqrt{\bar{n}}$ and thus the standard deviation is given by eq. (2.2).

$$\Delta n = \sqrt{\bar{n}} \quad (2.2)$$

Different kinds of light can be classified according to the standard deviation in their photon statistics and the possibilities are:

- **super-Poissonian:** $\Delta n > \sqrt{\bar{n}}$
- **Poissonian:** $\Delta n = \sqrt{\bar{n}}$
- **sub-Poissonian:** $\Delta n < \sqrt{\bar{n}}$

Super-Poissonian light has a broader distribution following from larger variations in the intensity and this is the case for classical light sources like black bodies. Sub-Poissonian light on the other hand has a distribution which is narrower than the distribution of a Poissonian source. Sub-Poissonian light is also called non-classical light since it is more narrow than the best imaginable classical light which would be a perfectly coherent electromagnetic field. Therefore, sub-Poissonian light has no classical equivalent.

Thermal light (i.e. from a black body), if only one single mode is considered, will follow the Bose-Einstein distribution. However, if many modes are present or if there's only one mode but the time window of detection is long, the statistics of this light will also approach the Poissonian distribution [6].

2.2.1 Quantum theory of photodetection

Quantum theory gives a relationship between the variance of the photons in the light field $(\Delta n)^2$ and the variance of the photon count numbers from the detector $(\Delta N)^2$:

$$(\Delta N)^2 = \eta^2 (\Delta n)^2 + \eta (1 - \eta) \bar{n}. \quad (2.3)$$

This relation implies that if the incident light is Poissonian the output statistics will always be Poissonian no matter the quantum efficiency η . It also implies that if $\eta \ll 1$ any incoming distribution will become Poissonian in the output. This means that a detector with high quantum efficiency is needed if the photon statistics need to be resolved. With low efficiency photodetectors the photon statistics will thus always be Poissonian.

2.2.2 Effect of losses on photon statistics

Losses can be modeled as a beam splitter randomly losing photons in the light field according to a random sampling process. Detection inefficiencies can also be seen as a random sampling of which photons to detect. All of these random sampling processes contribute in making a sub-Poissonian light more Poissonian [6].

2.2.3 Electrons vs photons

Electrons and photons have quite different characteristics when considering their behaviour and emergent statistics. Since electrons are fermions they are not able to occupy the same quantum state and also tend to repel each other. This causes a stream of electrons to become naturally anti-bunched and exhibit sub-Poissonian statistics. Photons on the other hand are bosons and are free to occupy the same quantum state and they do not interact with each other which thus preserves any present statistics. A sub-Poissonian current source is thus easily achieved by using a resistor in series with a battery and as long as the voltage drop across the resistor is larger than $2k_B T / e$, the thermal noise contribution from the resistor is below the shot noise limit. If an LED with high quantum efficiency is driven with this current the generated photons will also exhibit sub-Poissonian statistics [6].

2.2.4 LEDs vs lasers as light sources

LEDs are in general less noisy compared to lasers since lasers are more sensitive to power instabilities and other noise sources. This means that most lasers have noise above the shot noise level for all frequencies and only special single-mode lasers with stabilization schemes can get down to the shot noise level. Therefore it is also easier to achieve sub-Poissonian light using LEDs [6].

2.3 Noise

Noise is something present almost everywhere. Noise is often unwanted and can be stochastic in nature but doesn't necessarily have to be completely random. It is often characterized according to its probability density function, e.g. if it has a Gaussian or Poissonian distribution, and according to its spectral density, e.g. if its white (completely flat) or pink (skewed towards lower frequencies). Technical noise is a generic term often used to refer to all the unwanted noise present in the system.

It is often convenient to talk about the ratio between the signal (in this project really the desired noise, i.e. shot noise) and the amount of unwanted noise. This ratio is called the SNR, signal to noise ratio.

Noise equivalent power (NEP) is an important metric for photodetectors. It is defined as the input optical power required to achieve a SNR = 1 over a bandwidth of 1 Hz. If input optical power for SNR = 1 is P_1 and Δf is the bandwidth of the detector it can be calculated using eq. (2.4) [7].

$$\text{NEP} = \frac{P_1}{\sqrt{\Delta f}} \quad (2.4)$$

2.3.1 Noise sources in photodiodes

For a silicon photodiode there are only three kinds of noise that has to be taken into account: thermal noise from the load resistor, shot noise from leakage current resulting from the reverse bias (explained further in section 2.4.2) and shot noise from the signal [8]. Possible background noise might also contribute. For this application the shot noise in the signal is the actual signal and source of entropy and the other noise sources are considered to be noise in this context.

2.3.2 Shot noise

Quantum electrodynamics states that light interacts with matter in quantized packets of energy, i.e. light can only be detected one photon at a time. This quantization results in inherent fluctuations in the photon detection rate and thus the generated photocurrent will also exhibit these fluctuations. The fluctuations manifest as noise and this is referred to as shot noise. The noise power of this noise is:

$$P = (\Delta i(t))^2 R_L \quad (2.5)$$

where R_L is the load resistance and Δi is the standard deviation of current fluctuations caused by the noise.

If Poissonian light is detected the photoelectron statistics will also be Poissonian and follow eq. (2.2) and since the photocurrent is proportional to the number of photoelectrons, the variance of the photocurrent will be proportional to the average photocurrent. By taking the Fourier transform of $i(t)$ you arrive at the relationship in eq. (2.6) where Δf is the frequency

bandwidth and e the elementary charge of each electron [6].

$$(\Delta i)^2 = 2e\Delta f \langle i \rangle \quad (2.6)$$

From this relationship it is also apparent that shot noise is flat in the frequency spectrum since there is no frequency dependency, i.e. shot noise is spectrally ‘white’. In practice however the detected noise starts to roll off at higher frequencies, typically starting from the frequency $1/\tau_D$ which depends on the response time τ_D of the detector. At low frequencies other classical noise sources are often present and completely drown the shot noise. In semi-classical theory it is impossible to get below shot noise and therefore it is often called the shot noise limit. The only way to get below this limit is to use sub-Poissonian light sources, i.e. non-classical light, and detectors with high quantum efficiency [6].

Just like in the photon statistics case, the photoelectron statistics from a photodiode with low efficiency will always be Poissonian and thus exhibit shot noise. This can be seen as originating from the stochastic character of photodetection. If shot noise from the actual light field is to be resolved, high quantum efficiency for the detector is required [6].

This is not only a phenomenon of photons and light fields since electrons also are quantized particles that constitute electrical current. Shot noise will therefore arise naturally in electrical current. This shot noise is however more easily suppressed since electrons are fermions and interact with each other. Usually this is the case for conductors or resistances where the electrons scatter and thermalize which leads to more thermal noise in the channel. Therefore if the origin of shot noise is light fluctuations, the fluctuations can instead be so strong that the suppressing effects in the electrical domain do not degrade the shot noise significantly. This might not necessarily be the case for mesoscopic systems like conductors with really small dimensions [9].

Photoconductors are an alternative source of shot noise. Shot noise from these components is sometimes referred to as double shot noise since both generation and recombination are Poissonian processes in a photoconductor. In a regular photodiode the recombination is instead deterministic since it occurs mainly at the contacts and this is in general not stochastic. Photoconductor will however contribute a substantial amount of flicker noise caused by conductance fluctuations [8]. The carrier lifetime in photoconductors also puts a limit on the response times and speed of detection.

Another way to think about the shot noise of an optical beam is to view the resulting noise as the interference between a noiseless optical beam and the zero-point vacuum fluctuations of the electromagnetic field. Because of this shot noise will be present both in the phase and amplitude of the light field when measuring it in a detector. In this way shot noise is an intrinsic noise that arises whenever light interacts with matter [8].

2.3.3 Thermal noise (Johnson-Nyquist noise)

Thermal noise can be derived from classical thermodynamics and arises from the fact that processes capable of dissipating energy will display thermal fluctuations. This means that components that can dissipate electrical energy, e.g. resistors or lossy capacitors, will be sources of thermal noise. A resistor at temperature T will transfer noise whose power over a 1 Hz bandwidth according to

$$p_n = k_B T \quad (2.7)$$

where k_B is the Boltzmann constant and to obtain the full noise power P_n this is integrated over the squared modulus of the network's transfer function as

$$P_n = k_B T \int_0^\infty |H(f)|^2 df. \quad (2.8)$$

This reduces to

$$P_n = k_B T \Delta f \quad (2.9)$$

when the transfer function is flat in the frequency domain [8].

For noise analysis of resistances it can be convenient to replace the resistance with its Norton or Thévenin equivalent by replacing it with a noise current source or noise voltage source together with an ideal resistor (that is noiseless). For the Thévenin model the open circuit RMS voltage noise e_N becomes

$$e_N = \sqrt{4k_B T R} \quad (2.10)$$

while for the Norton model the short circuit current noise i_N becomes

$$i_N = \sqrt{\frac{4k_B T}{R}} \quad (2.11)$$

2.3.4 1/f noise (flicker noise)

Noise that has power spectral distribution matching $1/f$ for low frequencies in the frequency domain is referred to as $1/f$ noise, but it is also known as flicker noise since this noise can also diverge quite a bit from a $1/f$ distribution. This noise originates from all kinds of sources like contamination migration on surfaces, conductance fluctuations in carbon resistors, migration of metal atoms in conductors etc. and is often also referred to as excess noise. The noise power of this kind of noise is proportional to i^2 in contrast to shot noise whose noise power density is proportional to i . Therefore the contribution of $1/f$ noise generally becomes worse for higher currents. Excess $1/f$ noise is often a symptom of bad and noisy components and can sometimes to some extent be mitigated by choosing components carefully. Metal film resistors (often called thin film for SMT components) have much less noise than the thick film variety which can be especially noisy for large resistance values (up to 30 dB lower flicker-noise compared to the thick film variety) [8].

2.3.5 Popcorn noise

Popcorn noise, also known as telegraph noise, manifests as stepwise random changes in the input voltage of some devices like amplifiers or transistors. It is also present in avalanche devices such as APDs and high-voltage zener diodes [8].

2.3.6 Avalanche noise

In an avalanche photodiode (APD) carriers are multiplied and thus amplified. This is the case both for photogenerated and thermally generated electrons. Because of this the accompanying shot noise is also amplified. This process is however not perfect, and a lot of so called avalanche noise is added in the process. This is because the underlying mechanism impact ionization is stochastic and adds further noise [7].

2.4 Photodetection

An immense array of applications require some kind of light detection and one of the most common detectors are photodiodes. Photodiodes are very similar to LEDs but instead of

emitting light, they are used to generate a current in response to impinging photons onto the diode. There is no internal multiplication gain in regular photodiodes and thus the generated photocurrent i_{pc} is given by

$$i_{pc} = \eta e\Phi \quad (2.12)$$

where η is the quantum efficiency of the photodiode, e is the electron charge and Φ is the photon flux. In a detector with $\eta = 1$ each photon will generate one photoelectron.

The square-law states that the output electrical power from an optical detector is proportional to the square of the input optical power. This arises from the fact that optical power is proportional to the photon flux and electrical power is proportional to i^2 . If a detector generates an EHP for every photon, the electrical current will be proportional to the photon flux and the electrical power then follows proportionally as the square of this. This in turn means that when comparing SNR the ratios on the electrical side will be the square of the ratios on the optical side since SNR is defined in terms of power and not amplitude [8].

Shot noise presents an upper bound of the SNR of the detector system according to

$$\text{SNR}|_{1 \text{ Hz}} = \eta N / 2 \quad (2.13)$$

where η is the quantum efficiency of the detector and N is the photon flux (i.e. photons/s). This is a fundamental limit that cannot be improved upon regardless of the detector having built-in amplification for instance [8].

Responsivity of a detector is defined as output current over input optical power (A/W) [8]. The expression for responsivity is shown in eq. (2.14)

$$\mathcal{R} = \frac{M\eta e}{h\nu} \quad (2.14)$$

where M is the multiplication gain in the detector, e is the electron charge and $h\nu$ is the photon energy. Note that the responsivity is also very dependent on wavelength.

2.4.1 Detector capacitance

The shunt capacitance, C_d , of the photodiode is almost always a big nuisance since it acts as a filter and severely limits the bandwidth of the detector. It will in essence shunt the generated photocurrent away from the rest of the detection circuit. This shunting is not an issue for very low frequency components of the current or if the diode is operated in a very high photon flux condition [8]. Since capacitance is proportional to the active area of the detector, detectors with larger surface area generally have higher and thus worse parasitic shunt capacitance. A model for a photodiode is shown in fig. 2.2.

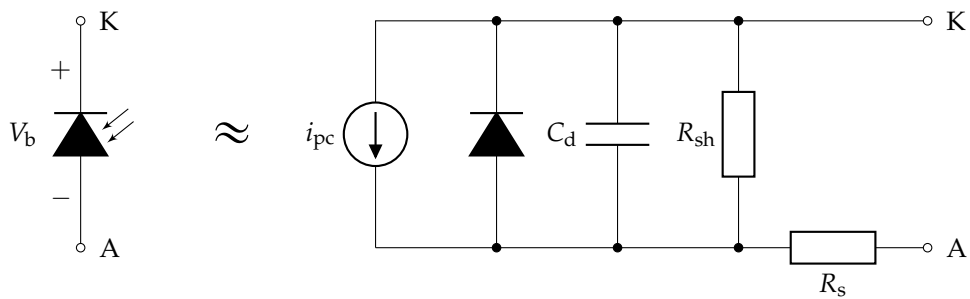


Figure 2.2: Approximate photodiode model with parasitic elements.

2.4.2 Reverse bias

The diode consists of a PN-junction which is formed by joining a P-doped and N-doped semiconductor. A schematic of this can be seen in fig. 2.3. The PN-junction also forms a depletion region (sometimes referred to as the space charge layer) between the two materials where mobile charges have been depleted. This depletion caused by the diffusion of charge carriers leaves behind the ionized dopant impurities within the depletion region. The ionized impurities in this zone create a built-in electric field which is also visualized in fig. 2.3. By applying a voltage across the photodiode from cathode to anode, i.e. in the reverse direction compared to normal LED operation, reverse biasing of the photodiode is achieved. The reverse bias widens the depletion region of the PN-junction which decreases the junction capacitance since the distance between the two regions is effectively increased [7]. This is useful for achieving higher bandwidth when using the photodiode as a high speed photodetector. The downside of applying a reverse bias to the photodiode is that a leakage current is created. This leakage current will create a DC offset error in the output signal and shot noise from the leakage current will also contribute to the overall noise. The leakage current is strongly dependent on temperature and more or less proportionally follows $\exp(-E_g / k_B T)$ where E_g is the band-gap of the semiconductor, k_B is the Boltzmann constant and the temperature T . For an InGaAs device this can be 8%/K whereas for a silicon photodiode it can be as large as 16%/K [8].

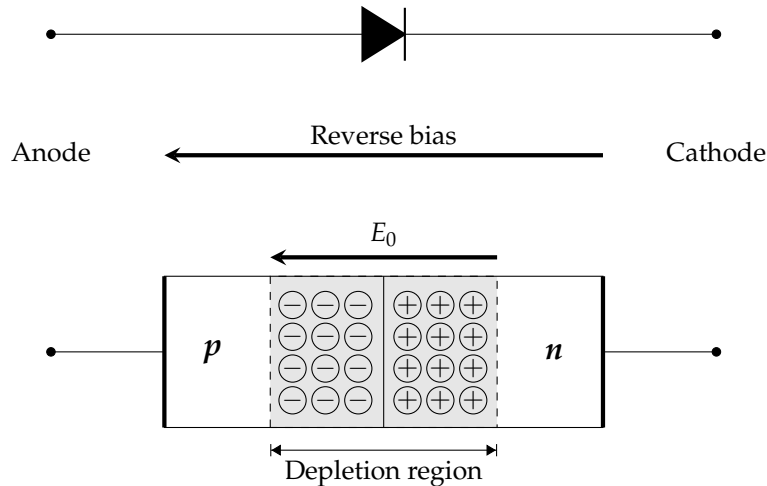


Figure 2.3: Illustration of how the PN-junction relates to the diode and where the depletion region is located. The electrical field resulting from the reverse bias and the built in field E_0 are also shown. The solid line in the middle is where the two differently doped semiconductors are joined, sometimes called the metallurgical junction. The regions outside the depletion region are referred to as neutral regions.

The reverse bias also increases the electric field strength in the depletion region which increases the speed of the charge carriers in the semiconductor material [8].

2.4.3 The LED as a light source

For visible light the red LEDs are the most efficient but the infrared LEDs are far more efficient and can have quantum efficiencies of around 0.4 [8]. As continuum sources, LEDs are fairly narrow-band but still have very short coherence lengths (on the order of 100 μm) which is much worse than lasers but still a lot better than other continuum sources like tungsten bulbs.

When varying the driving or bias current for phosphide LEDs they suffer very small spectral shifts and the output power is linearly proportional to the driving current except at very low driving currents (below 10 μ A [8]) where it rolls off due to a decrease in efficiency. Nitride LEDs however lose efficiency at high driving currents and also exhibit a substantial blue shift in their spectral output. Both the wavelength and efficiency of an LED is dependent on temperature. Typical LEDs are not that fast and can only be modulated at frequencies on the order of a few MHz.

When driving an LED with too high current the generated photons will exhibit quite a lot of $1/f$ noise. The cause of this is likely that the material deteriorates with junction damage and e.g. defect propagation under this stress. At high driving currents conductance fluctuations of the LED can dominate over other noise so a stable current source is beneficial [8].

2.5 Design of the photodiode amplifier

A photodiode amplifier can be realized in many ways and the design choice should be governed by the required characteristics for this application. Generally some important characteristics of amplifiers in photodiode applications are [10]:

1. linearity
2. offset
3. noise
4. bandwidth

It isn't immediately obvious that linearity is important in this application, but in order not to skew or bias the sampling of the quantum system it is beneficial to have a linear response if possible. It could be argued that the expected variations in photon flux are small and thus a perfectly linear response might be irrelevant since we are operating in such a small range where the response can be approximated as linear. If possible, it is better to try to preserve linearity though.

Noise is arguably one of the most important characteristics for this application since we want a high SNR for the noise (which is really our desired signal in this case) from the quantum system we are trying to sample.

Since high throughput is desirable for random number generation, and in order to sample the quantum noise with high temporal fidelity, a high bandwidth for the whole amplifier chain is crucial. In practice this means a bandwidth on the order of a couple of MHz to be competitive in this application.

The biasing of the diode has a big effect on its operation and characteristics. An unbiased photodiode is often said to be operating in photovoltaic mode while a reversely biased photodiode is sometimes said to be operating in photoconductive mode. It is better to just refer to it as operating with reverse bias since it is otherwise easily confused with photoconductors.

The photodiode will generate a photocurrent upon illumination and to work with this signal in a practical way it needs to be converted into a voltage. The photodiode signal can be monitored in two principally different ways, either voltage or current monitoring. Voltage monitoring puts a high load impedance on the diode and the photocurrent is intrinsically converted by the photodiode itself into a voltage across the diode's two pins. This is referred

to as operating the diode in photovoltaic mode and the generated voltage can be monitored and amplified by an operational amplifier. The other option is to present a close to zero load impedance to the diode and instead let the monitoring circuit sink the generated photocurrent. This way the circuit measures the photocurrent at the same time as keeping the diode in a low load-impedance environment [10]. Both of these alternatives are presented in fig. 2.4.

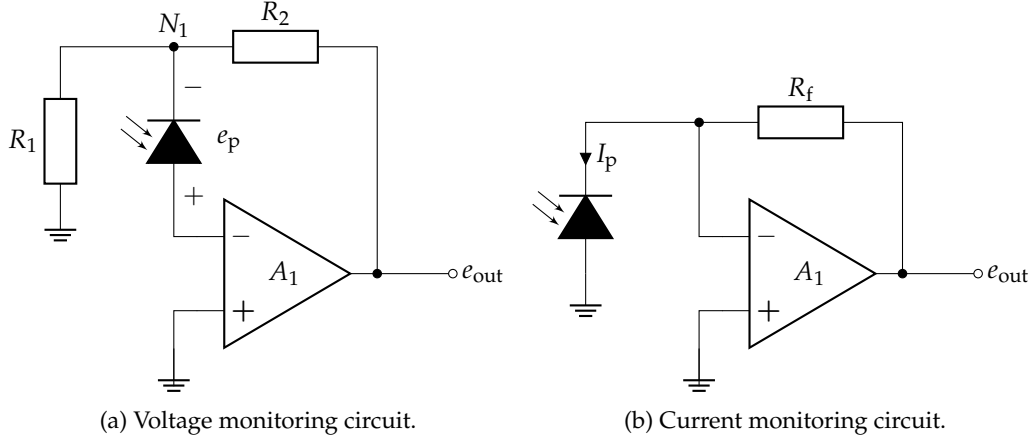


Figure 2.4: Alternative circuits for monitoring signal from photodiode.

The photodiode in the voltage monitoring circuit (fig. 2.4(a)) will upon illumination develop a voltage e_p over its terminals and the amplifier will try to compensate for this changed potential at its inverting input by driving its output to affect the voltage at node N_1 . This way the amplification will correspond to the voltage divider created by R_2 and R_1 according to the relation $e_{\text{out}} = -(1 + R_2/R_1)e_p$ [1].

In the second circuit (fig. 2.4(b)) the virtual ground created by the op amp at its inverting input presents a close to zero load impedance to the diode. The amplifier will continuously change the output voltage in order to push the photocurrent created by the photodiode through the feedback resistor. The developed voltage at e_{out} will thus be the photocurrent amplified by the value of the resistor according to eq. (2.15) (where $I_p = i_{\text{pc}} + I_L$ is the photocurrent i_{pc} plus leakage current I_L) and the amplification is simply R_f [10].

$$e_{\text{out}} = R_f I_p \quad (2.15)$$

In the photovoltaic domain the voltage e_p has a logarithmic relation to the photon flux ϕ_p according to

$$e_p = V_T \ln \frac{r_\theta \phi_p}{I_D} \quad (2.16)$$

where I_D is the dark current and $V_T = k_B T / q$ is the thermal voltage. The response of the photodiode, r_θ , determines the relation between the photon flux ϕ_p and photocurrent i_{pc} according to

$$i_{\text{pc}} = r_\theta \phi_p. \quad (2.17)$$

Looking at eq. (2.16) and eq. (2.17) it is evident that it is far better to choose current monitoring of i_{pc} instead of voltage monitoring e_p if you want to achieve linearity. It also achieves better offset and bandwidth characteristics than the voltage monitoring alternative [1].

The current monitoring circuit also removes voltage swing around the photodiode which otherwise modulates the responsivity r_θ which leads to yet another source of non-linearity

[1]. Having the signal voltage over the photodiode, as is the case for the voltage monitoring amplifier, also has the drawback that junction capacitance inside the photodiode will severely shunt the signal current for higher frequencies leading to an often significant bandwidth limitation [1].

This means that a transimpedance amplifier (TIA) used to convert the photocurrent into an amplified voltage is the most suitable first stage in the amplifier chain for this application.

2.5.1 Noise analysis of photodiode amplifier

The noise behaviour of the TIA circuit is quite complex. The basic sources of technical noise are:

1. feedback resistor (R_f) noise
2. amplifier input noise current (i_{ni})
3. amplifier input noise voltage (e_{ni})

The amplifier input voltage noise exhibits gain peaking for high frequencies. This mainly results from the high feedback resistance and diode capacitance. Other aspects like the parasitic capacitance of the feedback resistance and characteristic $1/f$ response of the input voltage noise further complicates the analysis. The noise analysis can be simplified somewhat by dividing the analysis into different frequency regions shown in fig. 2.6 [1].

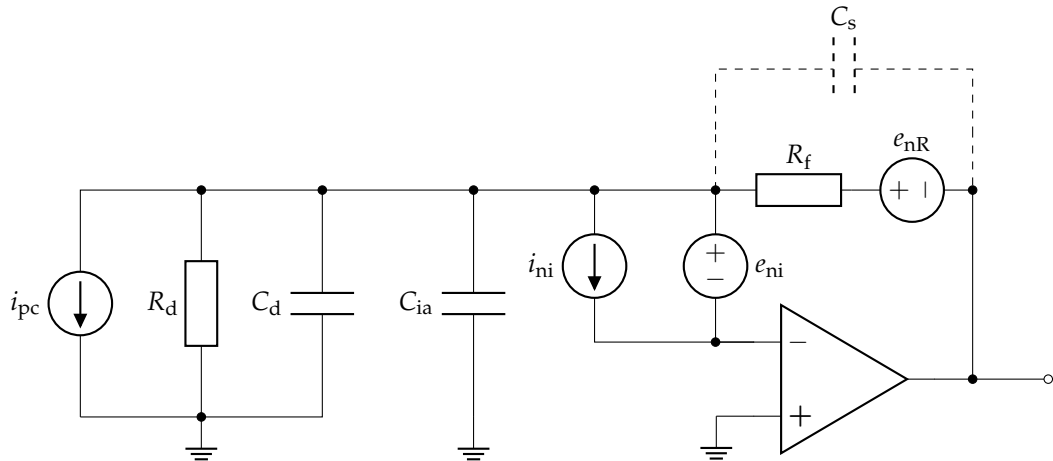


Figure 2.5: Noise model of photodiode amplifier with noise sources and parasitic elements.

In fig. 2.5 a noise model from [1] is shown with the photodiode modeled as a current source together with its impedance. The resistance R_D is the total resistance resulting from R_{sh} and R_s in fig. 2.2. The capacitance C_{ia} is the sum of the common mode C_{icm} and differential mode capacitance C_{id} for the operational amplifier. The total input capacitance C_i of the amplifier then becomes:

$$C_i = C_d + C_{id} + C_{icm} \quad (2.18)$$

where C_d is the diode capacitance.

The noise voltage e_{nR} originates from the thermal noise of the resistor and has a spectral density according to eq. (2.19).

$$e_{nR} = \sqrt{4k_B T R_f} \quad (2.19)$$

The noise sources i_{ni} and e_{ni} represent the input noise current and input noise voltage of the operational amplifier respectively. The noise current i_{ni} really represents the shot noise of the input bias current I_{B-} at the inverting terminal and has a noise current density according to eq. (2.20) where e is the elementary charge.

$$i_{ni} = \sqrt{2eI_{B-}} \quad (2.20)$$

This noise current i_{ni} is amplified by R_f and appears at the output. For amplifiers with very low input bias currents this contribution is however insignificant.

The noise voltage e_{ni} is maybe the more complicated source since its output noise e_{noe} is modulated by the capacitances as shown in eq. (2.21).

$$e_{noe} = \frac{1 + R_f C_i s}{1 + R_f C_s s} e_{ni} \quad (2.21)$$

All in all this produces a net output noise density according to eq. (2.22) where e is the elementary charge.

$$e_{no} = \sqrt{e_{noR}^2 + e_{noi}^2 + e_{noe}^2} = \sqrt{4k_B T R_f + R_f^2 2e I_{B-} + \left(\frac{1 + R_f C_i s}{1 + R_f C_s s} e_{ni} \right)^2} \quad (2.22)$$

In order to calculate the net output noise power the noise density has to be integrated over the whole frequency range while also incorporating the noise gain A_n as is shown in eq. (2.23).

$$E_{no}^2 = \int_0^\infty |A_n e_n|^2 df \quad (2.23)$$

The result of all this is that the added noise power varies over the frequency spectrum. The analysis of the noise voltage e_{noe} effects can be divided into different frequency regions as shown by Graeme [1] and the different regions are illustrated in fig. 2.6. The location of the different regions depend on amplifier characteristics like $1/f$ corner frequency f_f and amplifier input capacitance, but also on component values like the feedback resistance and parasitic capacitances in the circuit. The frequency f_{zf} is located where the gain peaking of the voltage noise starts. The region of constant noise gain begins at f_{pf} . Eventually the open loop gain A_{ol} of the amplifier starts to limit the noise gain and this starts at frequency f_i (given by eq. (2.26)) and the spectrum completely rolls off at f_c which is the unity gain of the operational amplifier. Expressions for these are given in eqs. (2.24) and (2.25). In these equations C_s is parasitic capacitance of the feedback resistance R_f and C_i is the input capacitance of the amplifier.

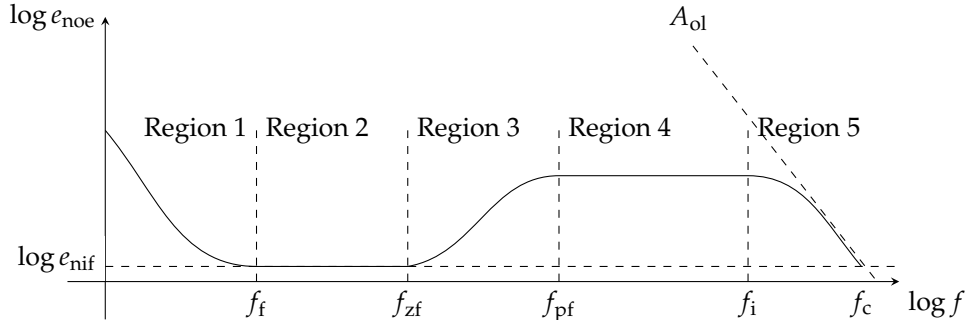


Figure 2.6: Noise spectral distribution of the noise voltage at the circuits output [1]

$$f_{zf} = \frac{1}{2\pi R_f (C_i + C_s)} \quad (2.24)$$

$$f_{pf} = \frac{1}{2\pi R_f C_s} \quad (2.25)$$

$$f_i = \frac{f_c C_s}{(C_i + C_s)} \quad (2.26)$$

All regions do not necessarily exist for all combinations of component values but if f_{zf} is larger than f_f , region 2 should provide a frequency band of minimal noise, i.e. a band with the same noise density as the amplifier voltage noise floor in that band.

When performing the integral in eq. (2.23) for the contribution of feedback resistance thermal noise e_{nR} , the result is that it is dependent on the feedback resistance R_f according to eq. (2.27) where BW_{th} represents the bandwidth (corresponding to the pole frequency f_{pf}) of this noise according to eq. (2.28) [1].

$$E_{noR} = \sqrt{2k_B T R_f \pi BW_{th}} \quad (2.27)$$

$$BW_{th} = \frac{1}{2\pi R_f C_s} \quad (2.28)$$

For op-amps with low input bias currents the overall noise is dominated by either the noise voltage of the op-amp, the thermal noise from the feedback resistance or the combination of these two. Which source is dominant depends on R_f and typically the voltage noise will dominate for resistances up to $10\text{ k}\Omega$ and the thermal noise will instead start to dominate when using R_f values above $10\text{ k}\Omega$. For even higher values of the feedback resistance (above $1\text{ M}\Omega$ the total noise will plateau and both the voltage noise and thermal noise will contribute as constants. Choosing an op-amp with low voltage noise will thus have no significance when the thermal noise is dominating [1].

2.5.2 Choice of operational amplifier for the TIA circuit

The characteristics listed in section 2.5 are also of importance when choosing the specific op amp to use. The amplifier will also inevitably introduce more noise sources and these have to be analysed and taken into consideration as well. It is desirable to pick an op amp with low input bias current since this current will in essence compete with the photocurrent from

the photodiode. The input bias current will also exhibit shot noise with very similar characteristics to the optically generated shot noise. Preferably this current should be substantially lower than the expected photocurrent in order to preserve the SNR. In practice this means op amps with input bias currents in the fA - pA range which often implies op amps with FET inputs [10].

Rail-to-rail amplifiers are quite popular because of their convenience in handling inputs and even output voltages that can be very close to the supply rails of the amplifier. Another nice characteristic is their relatively large voltage swing even on lower supply voltages like 3 to 5 V. One thing to be wary of however, is that rail-to-rail output amplifiers are susceptible to instability when loading their output. This is because of their very high output impedance (inherent for the type of transistor stage that is required in the output of rail-to-rail amplifiers). Thus rail-to-rail amplifiers typically have open-loop output impedance approximately an order of magnitude larger than similar non rail-to-rail amplifiers [8].

Input capacitance of the amplifier is important and was discussed in section 2.5.1. For example, FET type operational amplifiers are often attractive to use as they often have very low input bias currents. However, a compromise that is done here is that in order to decrease input noise the FET size is increased which in turn increases the input capacitance. Depending on the situation this increased input capacitance can cause excessive noise because of gain peaking resulting earlier in the frequency spectra even though the input noise was lower [1]. This trade-off can be extra important to consider for very low capacitance photodiodes.

Noise densities, both voltage and current, are also of high importance in low noise applications. Analysis of their effects on noise was presented in section 2.5.1. A very low voltage noise often mean higher current noise, larger bias currents (in bipolar amplifiers) and high input capacitance [8].

All in all some important characteristics to look for in a potential op-amp would thus be:

1. low input bias current
2. low noise
3. low voltage noise

2.5.3 Stability and bandwidth

It is very important to design an analog front-end that has stability in order to make reliable measurements on the noise. Stability is closely related to bandwidth since designs often have to make a compromise between bandwidth and stability. In order to have a front-end with high sampling rate and thus high bandwidth, it is essential to incorporate design techniques which increase stability and find the highest possible bandwidth without encountering instability issues.

Four main factors affect the bandwidth of the amplifier circuit [1]:

1. parasitic capacitance resulting both from PCB and the components
2. intrinsic bandwidth limit from op amp
3. phase compensation (often needed to stabilize the photodiode TIA circuits)
4. response time and thus frequency limit of photodiode

A capacitance parallel to R_f (which always exists for a physical resistor) will at high frequencies shunt the photocurrent through this capacitance instead of through the feedback resistance. This attenuates and limits the bandwidth at high frequencies. This effect can be beneficial though since this shunting can stabilize the amplifier and prevent oscillation. If the intrinsic stray capacitance (also called parasitic capacitance) of the feedback resistor isn't large enough to stabilize the circuit a capacitor should be added here.

In order to maximize the bandwidth of the circuit the stray capacitances have to be minimized as much as possible by utilizing various construction techniques. The stray capacitance C_s will introduce a pole at the pole frequency described by eq. (2.29) [1]. If this is the dominant pole in the circuit the amplitude characteristic will have a -3dB bandwidth limit at this frequency. It can also be noted that higher feedback resistances R_f also will affect this bandwidth limit in the same way as the capacitance by affecting the location of this pole. Thus this bandwidth limitation is often dominant in high gain circuits with high R_f .

$$f_{\text{pole}} = \frac{1}{2\pi R_f C_s} \quad (2.29)$$

Capacitive loading can also cause stability issues. This is because it introduces further phase lag in the feedback path. This phase lag can at a sufficiently high frequency create conditions for oscillation and the amplifier could start to oscillate. There are amplifiers referred to as unconditionally stable that have a sufficiently small feedback that prevents this from happening. It is recommended to use an unconditionally stable amplifier on inputs or outputs where you're not in total control of the potential loads. Amplifiers without this built in compensation circuitry can be faster at the cost of them not being unity gain stable and are often called decompensated op amps [8].

2.6 Signal to noise ratio for shot noise and thermal noise

The output voltage depending on the input signal (which is shot noise in this work) is given by eq. (2.15). The output thermal noise instead depends on R_f according to eq. (2.19). By taking the ratio of these two voltages you arrive at eq. (2.30)

$$\text{SNR}_{\text{shot,thermal}} = I_p \sqrt{\frac{R_f}{4k_B T}} \quad (2.30)$$

and thus the SNR increases with the square root of the amplification. This is somewhat simplistic though since increasing R_f will affect both the bandwidth and also voltage noise gain peaking (as discussed in section 2.5.1).

Method

This chapter describes how the prototype was implemented and then evaluated. The prototype itself consisted of a handmade circuit board which was placed inside a shielding metal box that was also constructed during the project. This chapter also covers how the evaluation of the prototype was performed and how the measurements were made. Whenever conducting measurements an optically opaque blanket was used to cover up the measurement box to further shield it from stray light from the outside. All measurements were performed using a Rohde & Schwarz RTB2004 DSO. The driving currents for the measurements were generated with a Keithley 2401 SourceMeter. Measurement campaigns were automated using VISA commands sent using Python to control the instruments and save sampled data.

3.1 Design

This section describes the design of the electro-optical front-end that was constructed during the project.

3.1.1 Optical front-end

The optical part of this generator was simple as it only consisted of an LED coupling light to a photodiode by roughly aligning them and placing them a few millimeters apart. This coupler could be enclosed to isolate it from stray light, but this was not done as the whole measurement box was instead covered. It was thus assumed that no other light than the light from the LED was present inside the measurement box. The resulting construction can be seen in fig. 3.2.

3.1.2 Electrical front-end

The circuit that was designed for the project consisted of an emitter (a Kingbright L-7103F3BT LED), a detector (a Vishay TEFD4300 silicon PIN photodiode) and the amplifier (an Analog devices LTC6268 current FET-input op-amp). Other than these main electronic components some bias circuitry for the photodiode and power supply for the amplifier were added. The resistors were all thinfilm of SMT type (i.e. really metal film) in size 0603. The thinfilm variety was used since they have much less noise compared to carbon or thickfilm resistors (discussed further in section 2.3.4). The final circuit diagram can be seen in fig. 3.1.

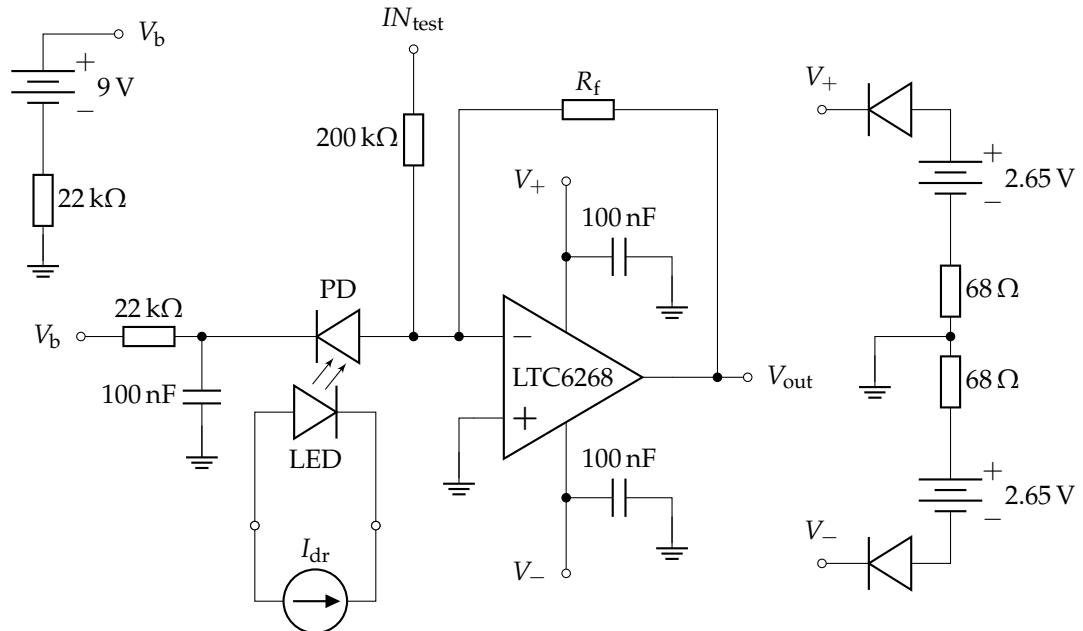


Figure 3.1: The schematic of the complete front-end including photodiode bias and power supply circuitry.

In fig. 3.1 V_b is the port used to apply bias voltage, IN_{test} is where the function generator is connected when measuring Bode plots, I_{dr} is where the driving current of the LED is supplied (galvanically isolated from the rest) and V_{out} is where the output is measured using the DSO. The power supply consisting of two battery packs at 2.65 V each are connected to V_- and V_+ .

The power supply circuitry includes current limiting resistors and silicon diodes to step down the voltage (and protect against reverse polarity) to achieve suitable supply voltages for the op-amp. The bias voltage V_b is also equipped with a passive low-pass filter with a cutoff of $1/2\pi RC \approx 70$ Hz. Decoupling capacitors are also added close to the supplies of the op-amp.

3.2 Implementation

The construction of the main prototype involved constructing both the prototype circuit board as well as the shielding Faraday cage that the prototype was placed inside of when carrying out measurements.

3.2.1 Measurement box

The box was constructed from a cast aluminium alloy box with a flat lid. Holes were drilled in the side of the box to allow pass-throughs of coaxial cables by installing SMA connectors in the holes. On the inside the coaxial cables from the SMA connectors led to UFL connectors for convenient attachment onto the DUT. Some connectors were grounded to the box itself while others were electrically insulated from the box with electrical tape to create galvanically isolated inputs for e.g. driving the LED. The box was dimensioned and constructed in order to enable similar measurements in the future that require low environmental noise to avoid interference.

3.2.2 Prototype circuit board

The main prototype circuit board was constructed using a method inspired from the Manhattan prototyping technique. Small islands of copper laminate were fastened using hot glue on top of a large copper board laminate forming a continuous ground plane. The electrical circuit was then realized by placing the components and thin enamel copper cables in between these islands and ground plane. Sometimes larger cables were used to route paths of the circuit across the board. Most components used in the prototype were of SMD type while some components associated with the power supply were of leaded variety. The IC was placed upside down ("dead bug" style) for more room when soldering the very thin enamel copper leads to the pins of the chip which can be seen in fig. A.3 in the appendix.

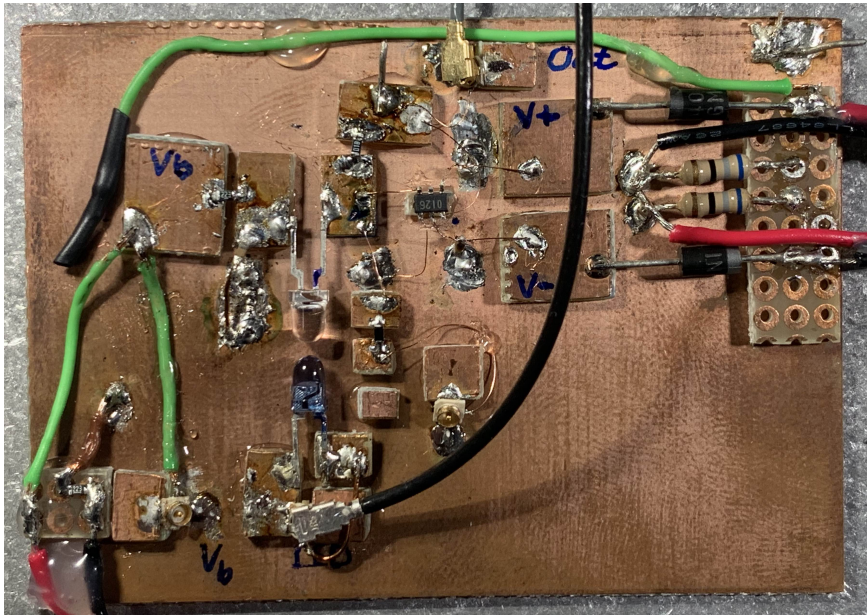


Figure 3.2: The complete prototype circuit board with amplifier and an LED in blue directed towards the transparent photodiode.

3.2.3 Choice of component values & filter parameters

Following from the noise analysis in section 2.5.1, region 2 in fig. 2.6 is assumed to have the least amount of noise. This region will be filtered out digitally during postprocessing in hope of achieving a signal with the least amount of technical noise. To perform this filtering, the lower and upper frequencies need to be determined. Since the LTC6268 amplifier has a $1/f$ corner at 80 kHz the lower frequency is taken to be this. The upper end f_{zf} of this region is calculated according to eq. (2.24) and the resulting optimal bandwidth selections are shown in table 3.1. These frequencies are then used to construct digital Butterworth bandpass filters of the 10th order that during postprocessing will filter out the signal present in these regions.

To obtain these frequencies some capacitances must be derived or estimated. The diode capacitance C_d which depends on the reverse bias is derived from the datasheet [11] of the photodiode and taken to be 1.1 pF since the reverse bias during measurement is 9.59 V. From the datasheet [12] of the amplifier, the differential mode capacitance $C_{id} \approx 100 \text{ fF}$ and the common mode capacitance $C_{cm} \approx 450 \text{ fF}$ are obtained. The feedback resistance stray capacitance is estimated to be $C_s \approx 500 \text{ fF}$. This results in a total input capacitance $C_i \approx 1.65 \text{ pF}$. This capacitance in turn yields the frequency regions presented in table 3.1 for the respective values of R_f when using eq. (2.24) to calculate values for f_{zf} . The last resistance of $1 \text{ M}\Omega$ yields an f_{zf}

which is lower than 80 kHz so for this amplification and its measurement data the frequency region 80 kHz to 10 MHz was used instead.

R_f	Frequency range for region 2	Cutoff (f_{pf})
1 kΩ	80 kHz to 74.0256 MHz	318.31 MHz
10 kΩ	80 kHz to 7.40256 MHz	31.831 MHz
22 kΩ	80 kHz to 3.3648 MHz	14.4686 MHz
47 kΩ	80 kHz to 1.57501 MHz	6.77255 MHz
100 kΩ	80 kHz to 740.256 kHz	3.1831 MHz
1 MΩ	80 kHz to 74.0256 kHz	318.31 kHz

Table 3.1: Frequency ranges corresponding to the lowest voltage noise contribution for the different amplifications R_f and the upper cutoff of the bandwidth (given by f_{pf}).

3.2.3.1 Silicon PIN photodiode

The photodiode utilized in the project was a TEFD4300 by Vishay. Some specifications [11] for this component is listed in table 3.2.

TEFD4300 PIN PD	Value	Test condition
i_d (dark current)	0.15 nA (Typ.)	$V_B = 10$ V (bias voltage)
V_{br} (breakdown voltage)	60 V (Min.)	$I_r = 10$ V (rev. current)
I_{ra} (reverse light current)	9 μA to 27 μA	$V_B = 5$ V
λ_p (peak wavelength)	950 nm	
$\lambda_{0.1}$ (spectral range)	350 nm to 1120 nm	
t_r, t_f (rise and fall time)	100 ns	$V_B = 10$ V, $R_L = 10$ kΩ
C_d (diode capacitance)	3.3 pF	$V_B = 0$ V, $f = 1$ MHz
	1.2 pF	$V_B = 5$ V, $f = 1$ MHz

Table 3.2: Si PIN photodiode TEFD4300 specifications [11]

From the datasheet it is found that operating the photodiode at a reverse bias of 20 V would yield a diode capacitance C_d of just 0.9 pF. A reverse bias of 9 V would yield a capacitance of approximately 1.2 pF. For all measurements a reverse bias of 9.59 V was used.

3.2.3.2 GaAs infrared LED

The emitter that was used in this project was the L-7104F3BT GaAs infrared LED by Kingbright. According to the datasheet it has a maximum DC forward current of 50 mA [13]. Care is taken not to come close to this maximum drive current during measurements. This was however not the limiting factor as the photodiode in all cases was saturated before getting near the limitation of the LED.

3.3 Evaluation

The front-end was evaluated in multiple ways. This section describes the different methods of evaluation. During the experiments the sourcemeter was used to generate the small driving currents for the LED and the oscilloscope was used to capture the resulting data.

3.3.1 Noise floor

To evaluate the technical noise in the system and the efficacy of the employed shielding strategies, frequency spectra for different configurations were recorded. These noise floors were captured using a DSO. The noise floor was recorded for different configurations to compare how the noise changes when, for instance, the sourcemeter is connected to the LED.

3.3.2 Transfer function of the amplifier

The transfer function of the electrical amplifier was obtained by creating a Bode plot using a DSO which is equipped with its own function generator. This Bode plot was however limited to 25 MHz so the transfer function could only be evaluated up to this frequency. In order to avoid oscillations for some component values and to ensure correct amplitudes in the transfer function both the signal from the built-in function generator and the output from the DUT was 50Ω -terminated.

3.3.3 Shot noise measurements

To evaluate the performance of the analog front end the operation of the amplifier is characterized for different amplifications. This was done by simultaneously measuring a DC-coupled and AC-coupled version of the output V_{out} , i.e. the coaxial cable first connected to a T-junction at the DC-coupled DSO channel and then connected to the AC-coupled DSO channel with a 50Ω termination at the end. The data were collected using a sample rate of approximately 41.66 MHz and both channels were recorded simultaneously.

To see that the amplifier correctly responds to changing photon flux the DC-coupled output signal V_{out} is sampled. Measurements are performed for the respective amplifications (by replacing the feedback resistance R_f) and data is collected while stepping the driving current I_{dr} of the LED. The final value for a measurement run is the arithmetic mean of the whole time series.

The data from the AC-coupled channel was used to evaluate the noise of the output signal and this channel could utilize higher gain since the DC offset is not present when AC coupling. The final measurement for each measurement run is the RMS value of the series.

The feedback resistance values (and thus amplifications of the TIA) used for both of these measurements are presented in table 3.3.

The applied driving current started off with smaller values as shown in table 3.4 and was then increased in steps of $50\mu A$ until a detected mean photocurrent (adjusted for amplification) of approximately $15\mu A$ to $20\mu A$ was obtained since this is close to the maximum reverse light current of $27\mu A$ for the photodiode.

3.3.4 Estimation of electron charge

The methodology [14] used to calculate the electron charge from the noise is to plot the variance against the mean photocurrent. The x-axis is rescaled according to eq. (2.6) so the slope

R_f
1 kΩ
10 kΩ
47 kΩ
100 kΩ
1 MΩ

Table 3.3: Tested values of R_f .

I_{dr}	
1 μA	100 μA
5 μA	150 μA
10 μA	200 μA
25 μA	250 μA
50 μA	300 μA
	350 μA
	450 μA
	500 μA
	...

Table 3.4: Applied driving currents I_{dr} of the LED during measurement runs.

of the plotted data will correspond to the electron charge. The quantity plotted on the x-axis is derived from eq. (3.1)

$$\langle V_{out}^2 \rangle = 2e\langle i_{pc} \rangle R_f^2 \int_0^\infty [g(f)]^2 df + V_A^2 = 2e\langle V_{out} \rangle R_f \int_0^\infty [g(f)]^2 df + V_A^2 \quad (3.1)$$

where $V_{out} = i_{pc}R_f$ (eq. (2.15)) is used. The argument $g(f)$ inside the integral represents the gain of each frequency in the spectrum. In this evaluation this is calculated from the transfer function of the Butterworth bandpass filter used to select a specific frequency region of the signal. The residual term V_A^2 represents noise from the amplifier and thermal noise.

By recording data and plotting the variance (square of the RMS) against the rescaled x-axis at different mean photo currents, an estimate q of the true electron charge e can be achieved.

Results & Discussion

In this chapter the results of the evaluation of the amplifier and characterization of shot noise sampling are presented. The results are also discussed immediately after the presentation of each result.

4.1 Noise floor of the complete system

The noise floor for the complete system was characterized using the oscilloscope and plotting frequency spectra of the different configurations. The configurations used were:

1. only oscilloscope (i.e. without connecting the prototype's output to the oscilloscope)
2. inactive amplifier (i.e. without V_+ and V_- connected)
3. active amplifier (i.e. with V_+ and V_- connected)
4. drive current of 0 mA
5. drive current of 0.5 mA
6. drive current of 1.2 mA

For the first three configurations the sourcemeter was not connected to the system. The resulting data is shown in fig. 4.1.

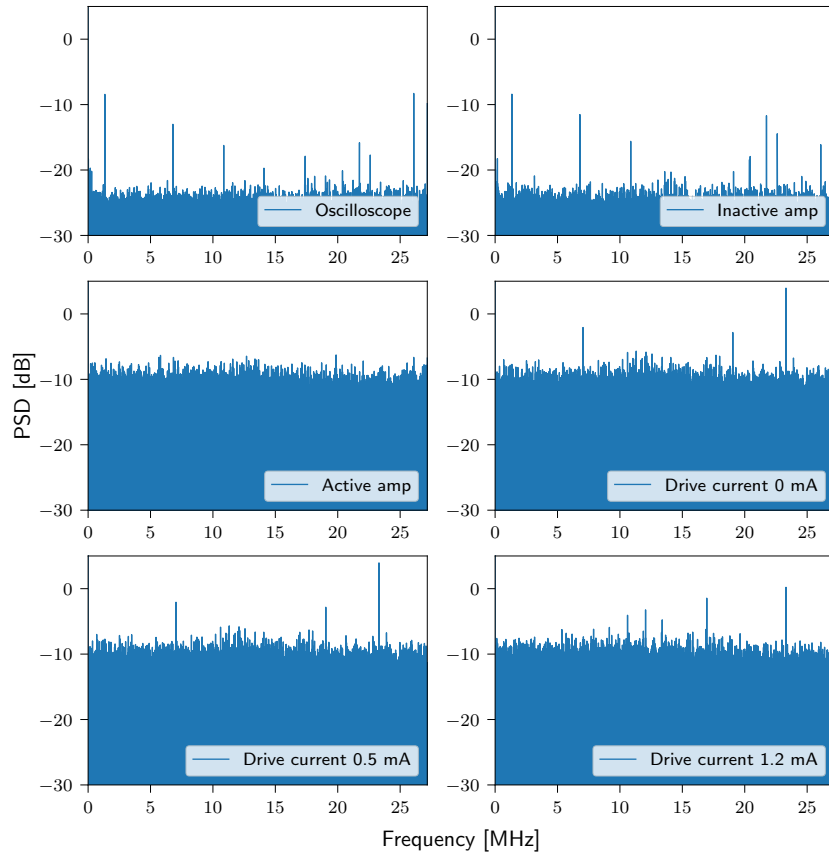


Figure 4.1: The noise floor of the system at different configurations.

The noise spectra appear quite flat and the noise floor is raised with approximately 10 dB when powering the amplifier. Some noise peaks at for instance 23 MHz seem to be introduced upon connecting the sourcemeter to the system. The noise doesn't appear to change much as the drive current is increased.

4.2 Transfer function of the amplifier

The transfer function obtained for the amplifier at different gain configurations is shown in fig. 4.2.

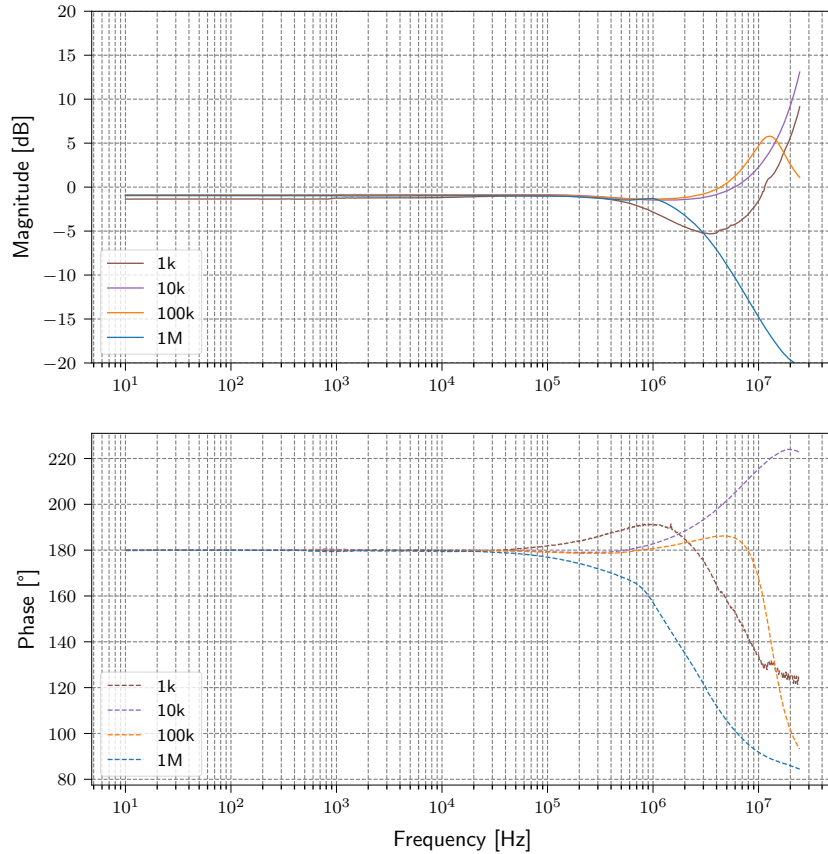


Figure 4.2: The transfer function of the amplifier between 10 Hz and 25 MHz for four different amplifications across the tested range. The magnitude is normalized to their respective expected amplifications.

For gains 1000 and 10 000 (corresponding to R_f of $1\text{ k}\Omega$ and $10\text{ k}\Omega$ respectively), the characterization seems to stop before measuring the true bandwidth. It can however be seen that some ringing or resonance is present at the highest frequencies. This could indicate that a compensation capacitor would be required in order to increase the stability of these lower gain configurations. The amplification of $10\text{ k}\Omega$ appears, however, to be flatter before rising at the highest frequencies. For a higher amplification of $100\text{ k}\Omega$ there is still some limited ringing but the decrease in gain before 25 MHz indicates that the bandwidth is around 30 MHz to 40 MHz. The bandwidth for $1\text{ M}\Omega$ is however clearly resolved at 1 MHz and it appears completely stable.

The phase for all configurations lie as expected at 180° since it is an inverting amplifier. Deviations are seen when the cutoff frequencies are approached. As discussed in section 2.5.2, the use of a rail-to-rail amplifier could have contributed to the instability and further stabilization techniques could have been employed.

4.3 Evaluation of the shot noise front-end

In this section results and discussion are presented for the measurements of the front end when it is generating noise.

4.3.1 Photodiode response to LED illumination

The measurement of the response of the photodiode amplifier is presented in figs. 4.3 and 4.4. In the normalized data in fig. 4.4 the slope is very similar for all amplifications but the curve for the amplification corresponding to a resistance of $1\text{ k}\Omega$ is offset below the others. In this figure the error resulting from the tolerance of the resistance values (1%) is presented as a lightly shaded area around the respective curves. The value on the y-axis in fig. 4.3 is obtained from the time average of the DC-coupled oscilloscope signal which measures V_{out} seen in fig. 3.1. In fig. 4.4 the voltage is instead used to derive the photocurrent i_{pc} and its mean so it can be plotted against the driving current I_{dr} .

The applied LED drive current is cut off when the photocurrent in the photodiode reaches close to the maximum specified photocurrent of the PD (as described in section 3.3), when the drive current gets too large (as described in section 3.2.3.2) for the driving LED (which never was the case) or when the amplifier gets close to saturating at its maximum output voltage.

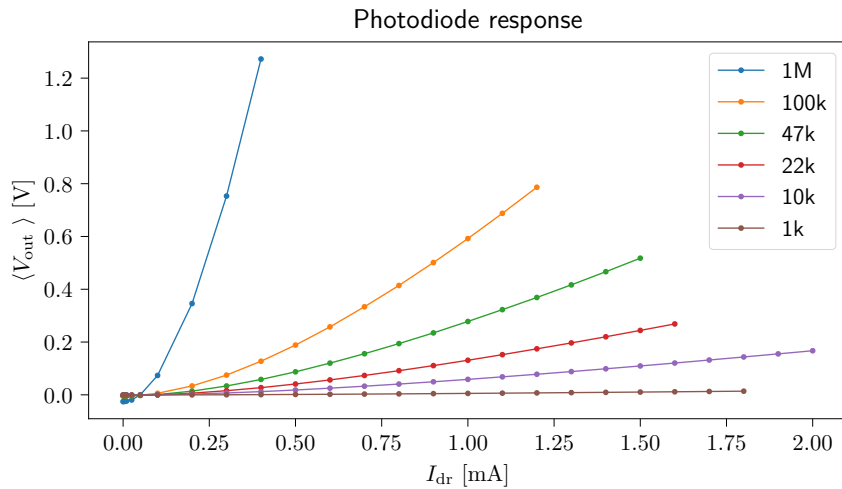


Figure 4.3: The response of the photodiode amplifier for different drive currents and different resistor values where $\langle V_{\text{out}} \rangle$ denotes the time-average of the amplifier output.

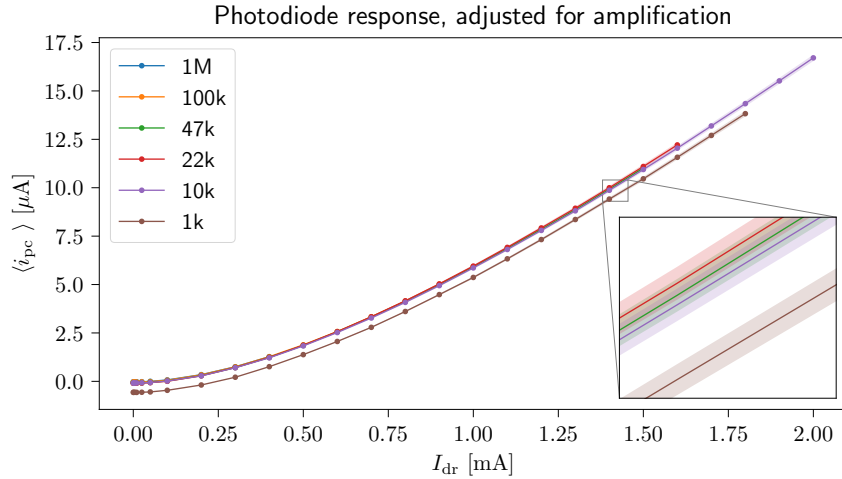


Figure 4.4: The response of the photodiode amplifier for different drive currents normalized using the respective amplifications (i.e. the same but rescaled data as in fig. 4.3).

Linear response in fig. 4.4 starts from approximately 0.7 mA of drive current. This indicates that a certain photocurrent is required before operating in a linear region of response. The response should be linear since photon flux increases linearly with applied driving current and the generated photocurrent is also proportional to the incoming photon flux.

4.3.2 Evaluation of RMS fluctuations in noise as function of drive current

The RMS of the AC-coupled measurement is plotted both against the LED driving current in fig. 4.5 and against the resulting mean value of the DC-coupled signal (which is normalized according to the resistance value).

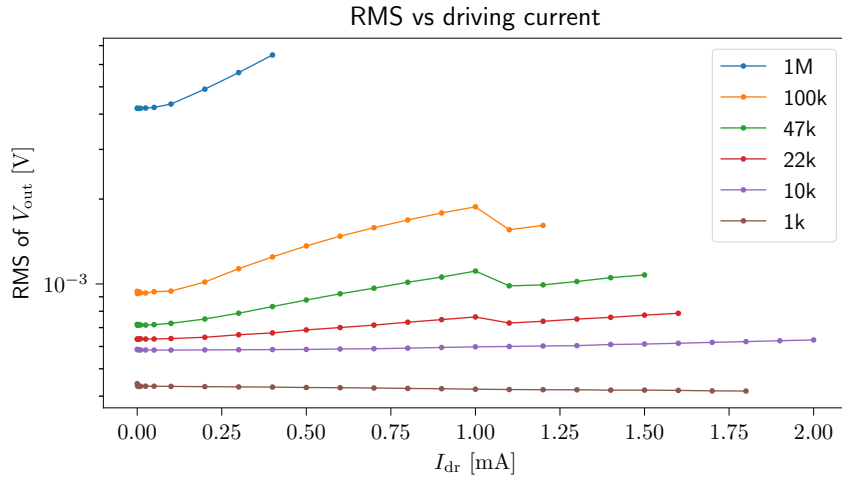


Figure 4.5: The RMS of the obtained noise plotted against the applied LED driving current for all amplifications.

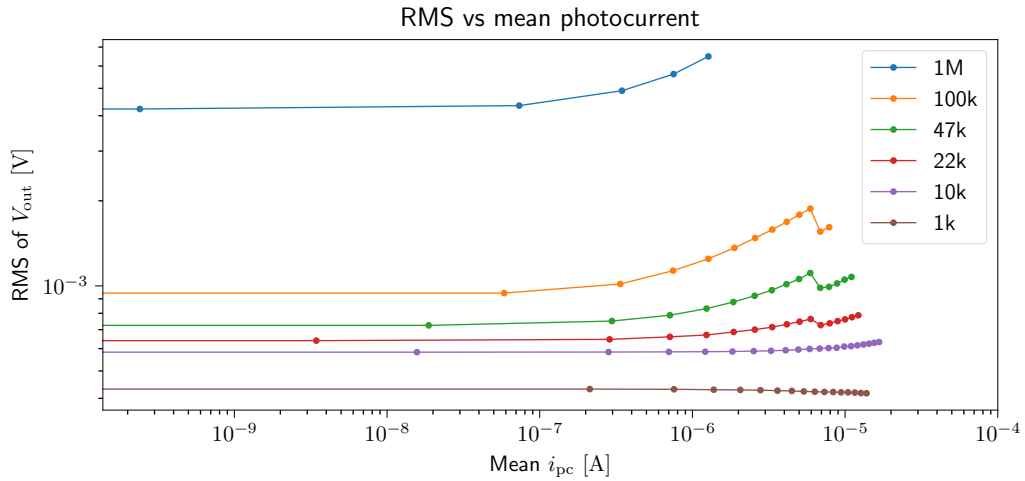


Figure 4.6: RMS of the V_{out} noise plotted against the resulting mean photocurrent i_{pc} .

4.3.3 Frequency spectrum analysis of noise

To analyse the noise in the frequency domain as a function of the amplifier gain, an FFT performed on the sampled data and the resulting frequency spectra are presented in this section. The purpose of this is to test how the noise depends on the component value chosen for R_F . It is also done to test whether the applied driving current affects the noise significantly.

4.3.3.1 Noise spectrum for zero LED drive current

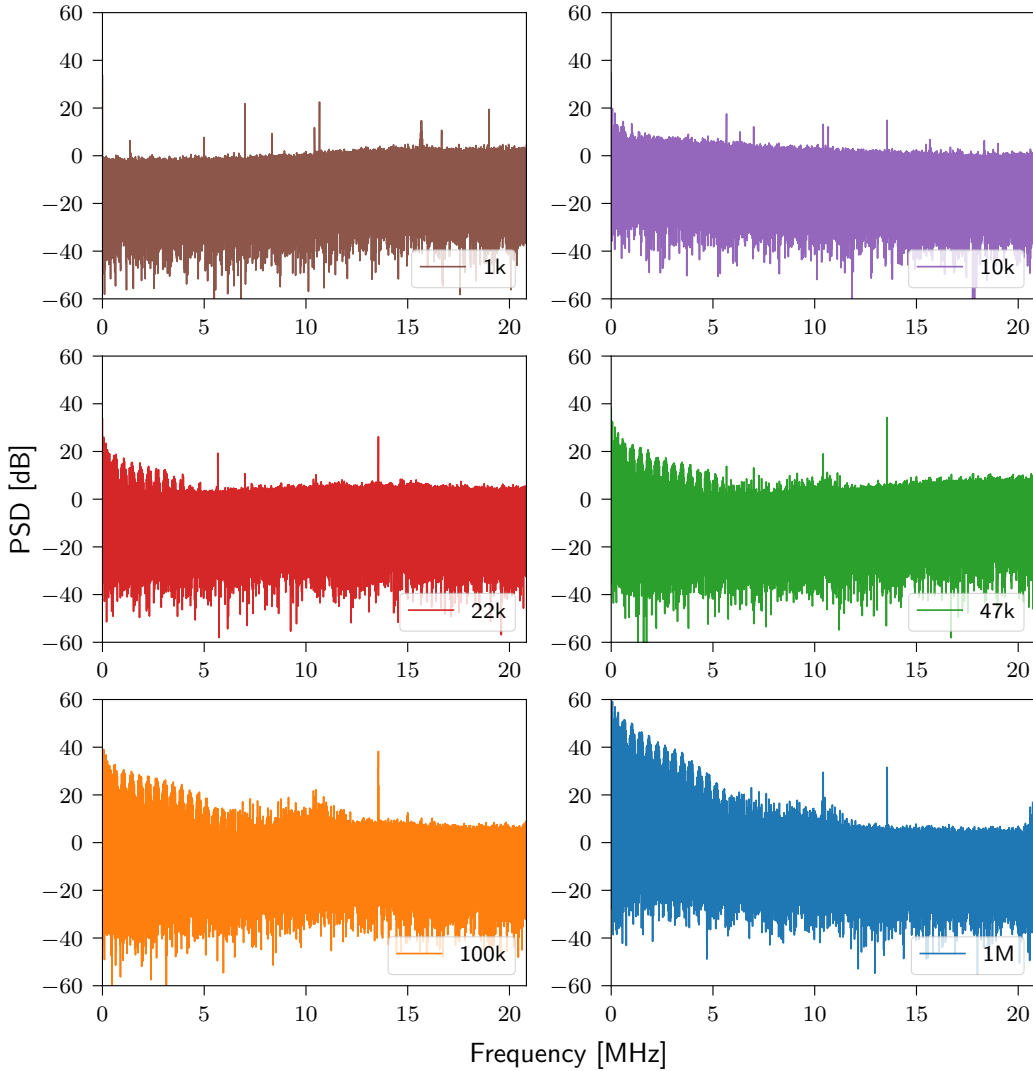


Figure 4.7: Spectrum using FFT for AC-coupled data for all gains at zero drive current of the LED (but with the sourcemeter turned on and connected to the system).

In fig. 4.7 it can be seen that there is a lot of pink noise below 8 MHz for all spectra from 22 k Ω to 1 M Ω . The cutoff frequency of this extra noise seems to increase for higher amplifications. Narrow peaks at 13.56 MHz is present for all gains except 1 k Ω . Another peak at 10.42 MHz is present for most of the spectra including the spectrum for 1 k Ω .

Noise peaks like this whose magnitude is independent of the gain used in the amplifier is indicative of the noise coming from a source external to the DUT and therefore couples into the circuit somewhere. It is however interesting to note that this coupling seems to only happen for the larger gains above 10 k Ω . This could be, for instance, radio interference from the outside environment or some lab equipment. This kind of noise should however have been mitigated by performing the measurements inside the shielding Faraday cage. It is thus unclear where this noise comes from.

4.3.3.2 Noise spectrum for low LED drive current

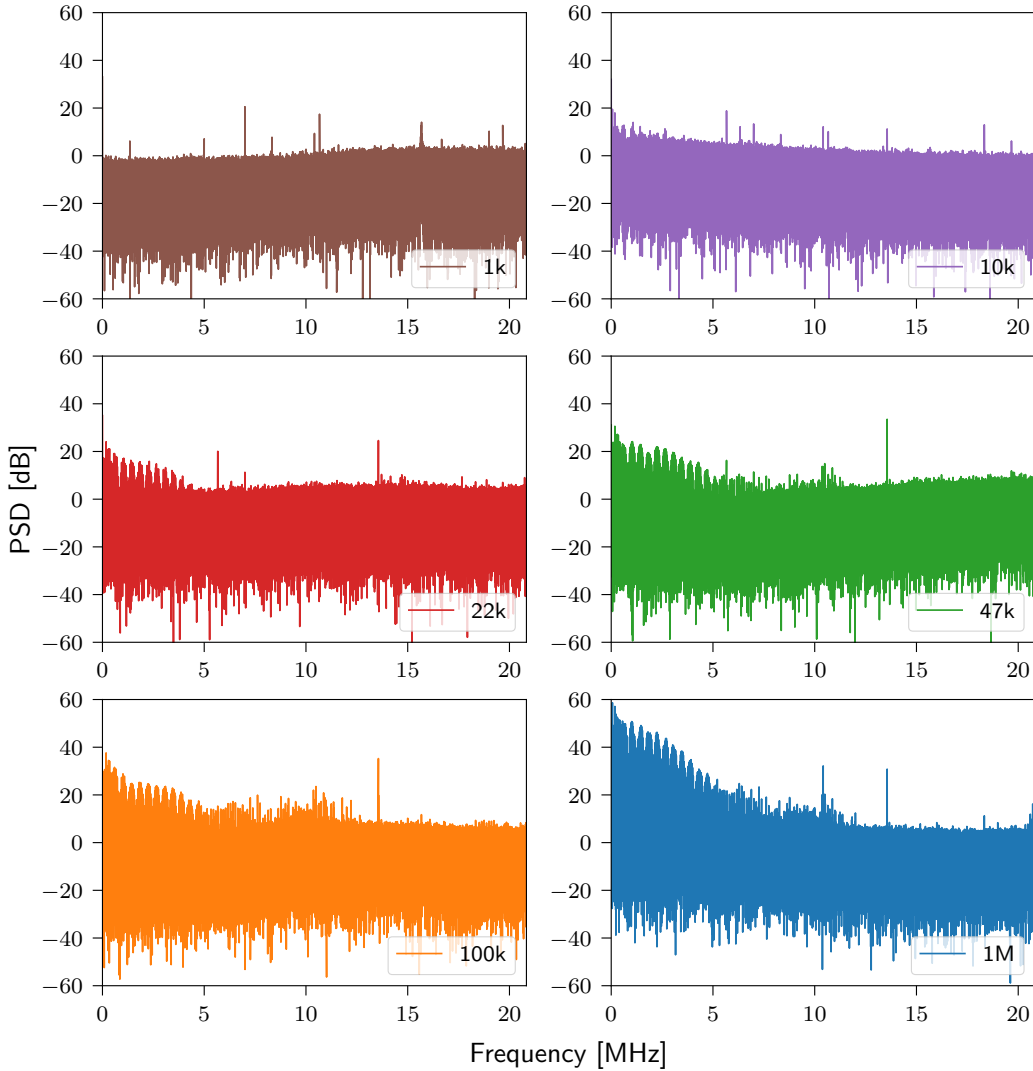


Figure 4.8: Spectrum using FFT for AC-coupled data for all amplifications at an LED drive current of $100\text{ }\mu\text{A}$.

When comparing fig. 4.8 with fig. 4.7, the behaviour for a small drive current of $100\text{ }\mu\text{A}$ is very similar to the case where there is no drive current. There is a slight increase in PSD for noise below approximately 8 MHz for all gains above $1\text{ k}\Omega$. This indicates that there is an insignificant change in noise when comparing zero drive current to low drive currents, i.e. the noise does not appear to change much for low photon flux.

4.3.3.3 Noise spectrum for high LED drive current

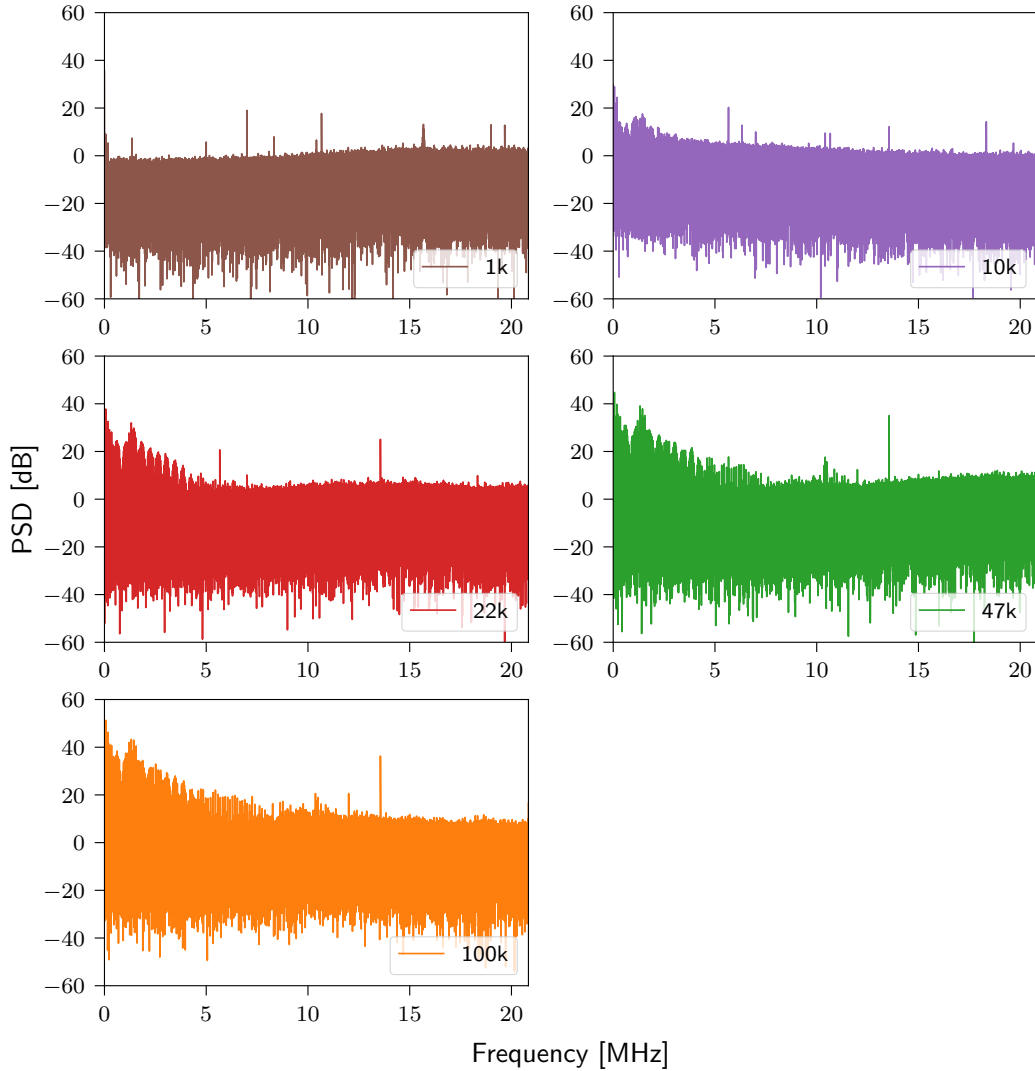


Figure 4.9: Fourier spectrum for AC-coupled data for all amplifications at an LED drive current of 1 mA. (There is no data for the highest amplification at 1 mA caused by saturation of the amplifier.)

When comparing fig. 4.9 with fig. 4.8, the behaviour for the larger drive current of 1 mA is similar to the case where lower drive current was used. The noise power has increased, especially for low frequencies at all amplifications.

When studying figs. 4.8 and 4.9 it is clear that there is a lot of noise present at frequencies significantly above the theoretical $1/f$ noise corner at 80 kHz. The only amplification (other than the $1\text{ k}\Omega$ case) that has considerably less noise than the others at the lower frequency range is the amplification corresponding to $10\text{ k}\Omega$.

4.3.4 Estimation of electron charge

In this section the results and discussion for the estimate q of the electron charge e are presented. The estimation of e is obtained using the slope of the presented figures. The vertical axis is the squared RMS (which corresponds to the variance of the signal since it is AC-coupled). The quantity on the horizontal axis uses the mean photocurrent, but it is rescaled using the squared feedback resistance R_f and the bandwidth of the signal to become the quantity $2R_f^2\langle i_{pc} \rangle \Delta f$, where $\langle i_{pc} \rangle$ is the mean value of the photocurrent. The bandwidth depends on whether band-pass filtering is applied to the signal. The correct value of q for the electron charge e should be $1.602\,176\,63 \times 10^{-19}$ C.

The slope should have the unit coulomb (C) which is equivalent to ampere-second (A s) and it can be seen that this is the case by dividing the units of the y-axis with the units of the x-axis.

4.3.4.1 Estimation using raw data

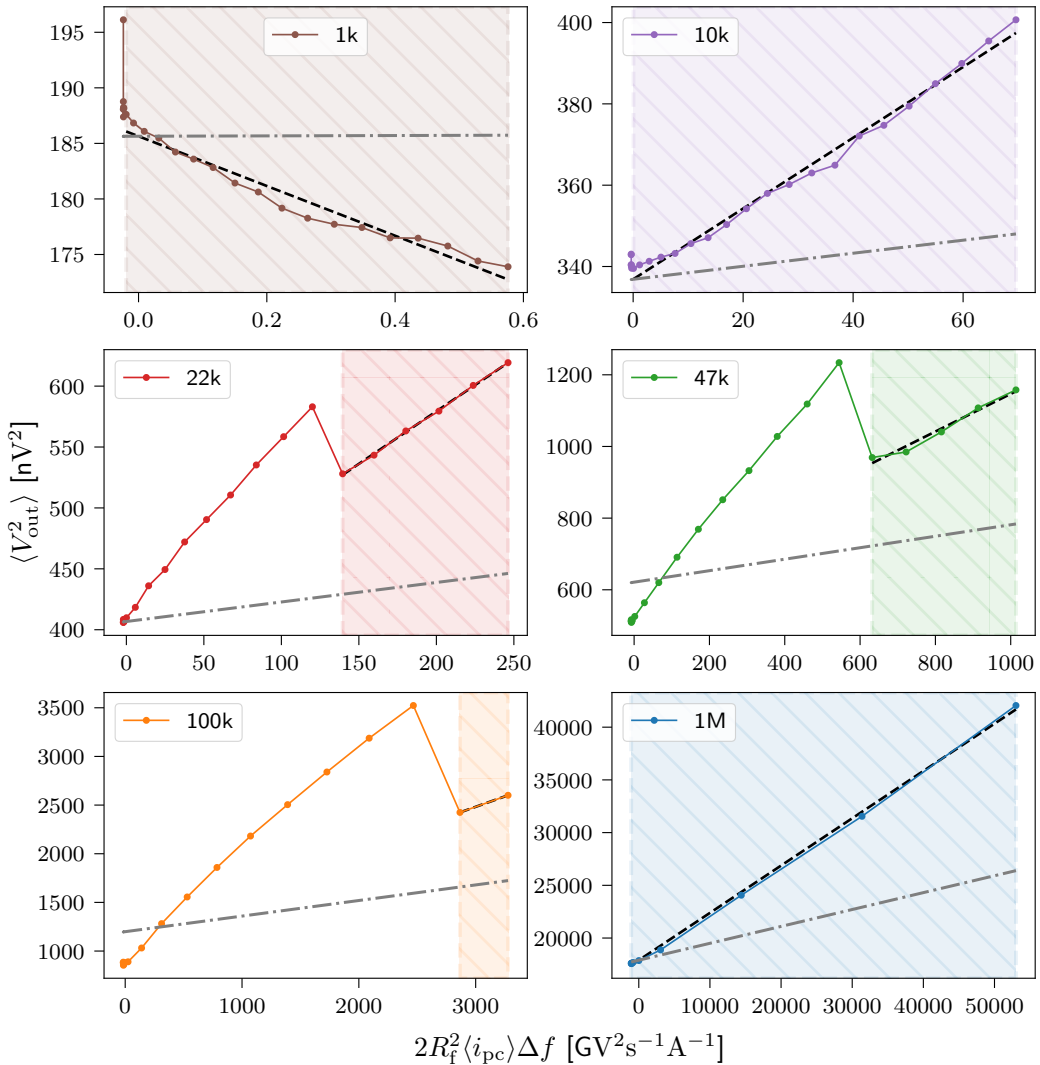


Figure 4.10: Rescaled squared RMS of V_{out} plotted against the resulting mean photocurrent i_{pc} . The slope should equal the electron charge, e , which is plotted in grey line with dashes and dots. The regression line used to obtain the estimate q is inside the shaded area and plotted in black with a dashed line.

The result of using no filtering when estimating e is presented in fig. 4.10. The corresponding estimates are presented in table 4.1. The slope is negative for $1\text{ k}\Omega$ which is obviously incorrect. The other estimates are in the correct order of magnitude and it can be seen that for some amplifications the slope is better at higher mean photocurrents. All estimates are higher than the true value of e which means that the variance in the signal is too large in relation to the mean photocurrent. This is likely caused by other noise present in the system which adds to the noise power and thus causes the RMS fluctuations to be too high in relation to the mean photocurrent.

All slopes are quite linear (except for the sudden jumps in $22\text{ k}\Omega$ to $100\text{ k}\Omega$) which also should be the case since the electron charge should be the same regardless of detected photocurrent. Since this corresponds so well with the sudden decreases in RMS when driving the LED with

R_f	Bandwidth [Hz]	Estimate q of e	Relative error
1 kΩ	20 833 292 Hz	$-2.238\ 54 \times 10^{-17} \text{ C}$	-14072%
10 kΩ	20 833 292 Hz	$8.701\ 62 \times 10^{-19} \text{ C}$	443%
22 kΩ	20 833 292 Hz	$8.628\ 48 \times 10^{-19} \text{ C}$	439%
47 kΩ	20 833 292 Hz	$5.255\ 03 \times 10^{-19} \text{ C}$	228%
100 kΩ	20 833 292 Hz	$4.276\ 94 \times 10^{-19} \text{ C}$	167%
1 MΩ	20 833 292 Hz	$4.486\ 10 \times 10^{-19} \text{ C}$	180%

Table 4.1: Resulting estimates of e when using raw data and the whole bandwidth of the sample data.

more than 1 mA, it is likely that this noise originates from the sourcemeter which generates the driving current and that it switches its electronics when it crosses this current threshold.

It is difficult to say why the slope has the wrong sign for 1 kΩ. It can however be noted that the data points are nested and sometimes with negative slope for currents very close to 0. It might thus be the case that the amplification and resulting signal from the photodiode is simply too weak when using a gain of 1000. If it was the case that too little illumination was used, the response should not follow the other curves in fig. 4.4, which currently clearly is the case, even though it has a slight negative offset. Another much more likely explanation is that the developed shot noise is completely below the technical noise floor. If this is the case, RMS noise should stay at the same level while the mean photocurrent increases and a negative slope would be observed. This is in agreement with what is observed in fig. 4.10 for 1 kΩ. If you look at the actual RMS data for this gain in fig. 4.6 though, it is seen that the RMS doesn't stay the same, it actually decreases slightly as photocurrent increases. This is very peculiar and the cause of this is not known.

4.3.4.2 Estimation using optimally filtered data

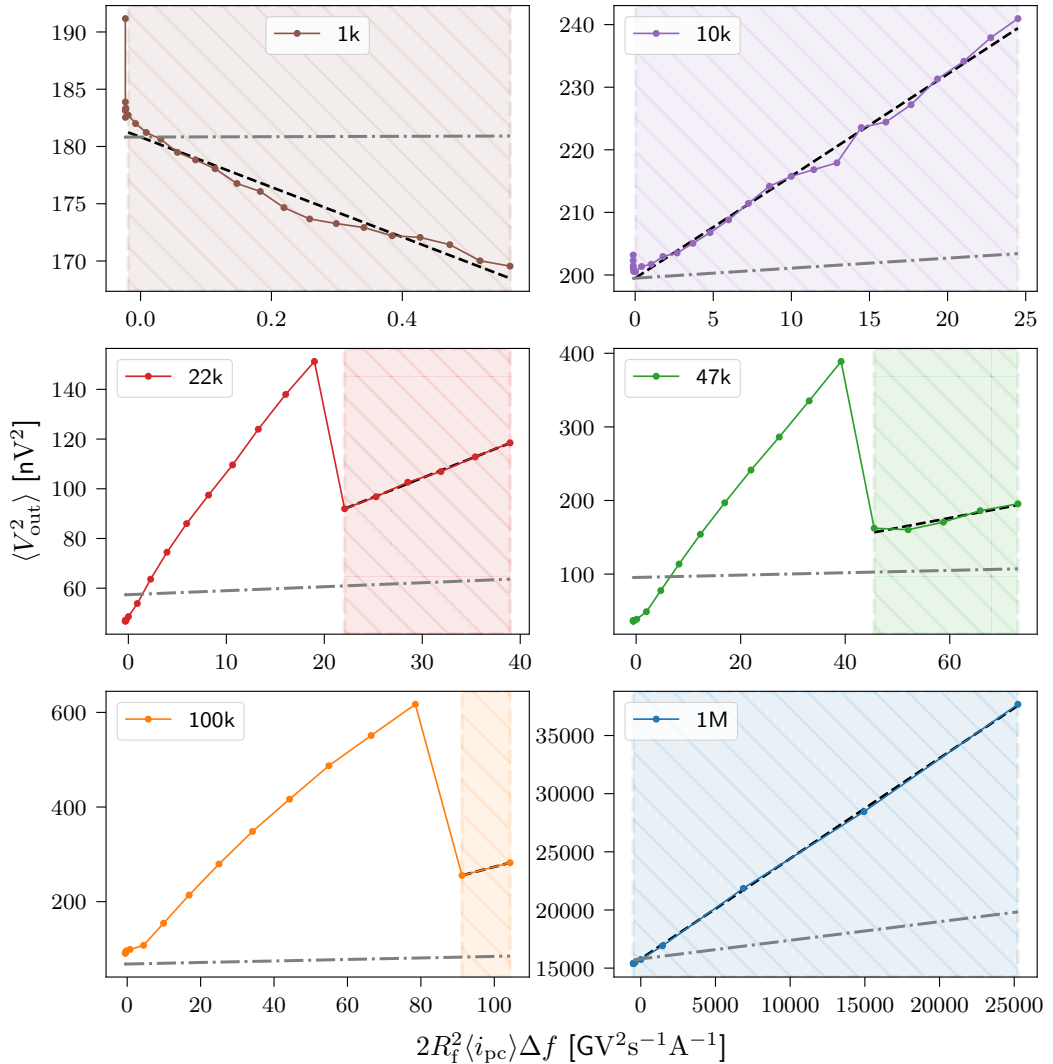


Figure 4.11: Rescaled squared RMS of V_{out} plotted against the resulting mean photocurrent i_{pc} . The slope should equal the electron charge, e , which is plotted in grey line with dashes and dots. The regression line used to obtain the estimate q is inside the shaded area and plotted in black with a dashed line.

The result of using the theoretically optimal filtering, as described in section 3.2.3 when estimating e is presented in fig. 4.11 and the corresponding estimates are presented in table 4.2. In these estimates the bandwidth is thus different for each amplification. The slope is still negative for $1\text{ k}\Omega$. The other estimates are one order of magnitude too large except for the $1\text{ M}\Omega$ measurement. The sudden jumps are also still present in the same way as for the unfiltered data above.

R_f	Bandwidth [Hz]	Estimate q of e	Relative error
1 kΩ	20 418 300 Hz	$-2.184\ 68 \times 10^{-17} \text{ C}$	-13736%
10 kΩ	7 333 395 Hz	$1.630\ 33 \times 10^{-18} \text{ C}$	918%
22 kΩ	3 296 190 Hz	$1.565\ 93 \times 10^{-18} \text{ C}$	877%
47 kΩ	1 500 965 Hz	$1.346\ 79 \times 10^{-18} \text{ C}$	741%
100 kΩ	662 960 Hz	$2.052\ 99 \times 10^{-18} \text{ C}$	1181%
1 MΩ	9 922 007 Hz	$8.628\ 99 \times 10^{-19} \text{ C}$	439%

Table 4.2: Resulting estimates of e when using optimally filtered data and the corresponding bandwidths.

4.3.4.3 Estimation using arbitrarily filtered data

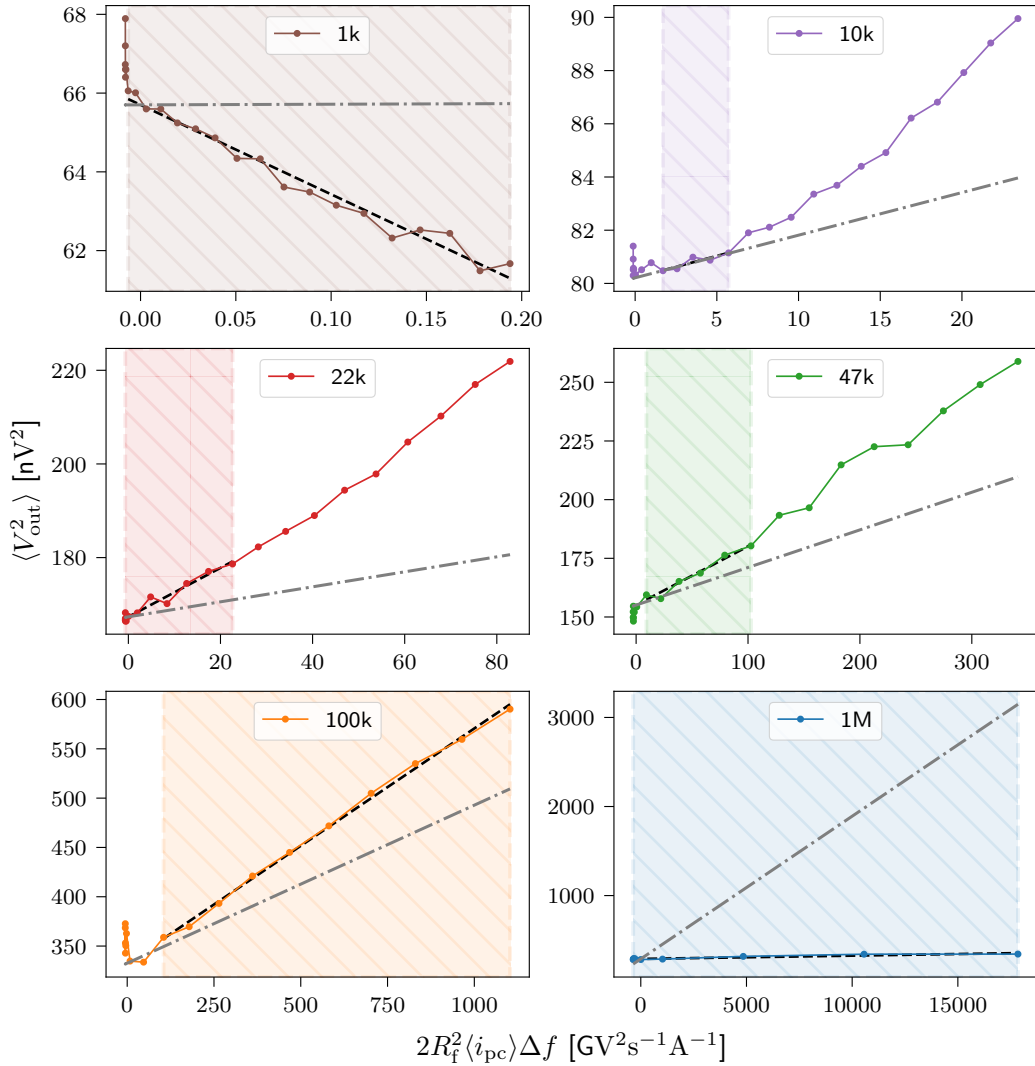


Figure 4.12: Rescaled squared RMS of V_{out} plotted against the resulting mean photocurrent i_{pc} . The slope should equal the electron charge, e , which is plotted in grey line with dashes. The regression line used to obtain the estimate q is inside the shaded area and plotted in black with a dashed line.

The result of using an arbitrarily chosen pass-band of 8 MHz to 15 MHz for the filtering when estimating e is presented in fig. 4.12. The corresponding estimates are presented in table 4.3. In these estimates the bandwidth and pass band is the same for all amplification. This could however have been chosen individually but in order to make the comparison more straightforward the same filtering was used for all.

Just like in the previous results, the slope is still negative for $1\text{ k}\Omega$. The other estimates are again all in the correct order of magnitude. The $1\text{ M}\Omega$ is the only one of these to underestimate e . The sudden jumps have now disappeared, but some of the curves show less linear behaviour. This seems for instance to be the case for $10\text{ k}\Omega$, $22\text{ k}\Omega$ and $47\text{ k}\Omega$.

R_f	Bandwidth [Hz]	Estimate q of e	Relative error
1 kΩ	7 011 576 Hz	$-2.271\ 91 \times 10^{-17} \text{ C}$	-14280%
10 kΩ	7 011 576 Hz	$1.645\ 14 \times 10^{-19} \text{ C}$	3%
22 kΩ	7 011 576 Hz	$5.229\ 26 \times 10^{-19} \text{ C}$	226%
47 kΩ	7 011 576 Hz	$2.503\ 75 \times 10^{-19} \text{ C}$	56%
100 kΩ	7 011 576 Hz	$2.379\ 88 \times 10^{-19} \text{ C}$	49%
1 MΩ	7 011 576 Hz	$3.651\ 41 \times 10^{-21} \text{ C}$	-98%

Table 4.3: Resulting estimates of e when using arbitrarily filtered data and the corresponding bandwidth. The same pass-band of 8 MHz to 15 MHz was used for all measurements.

By specifically choosing a region of the curve which corresponds best with the correct value of e , the best estimate that was achieved was $1.645 \times 10^{-19} \text{ C}$, which corresponds to a 3% relative error. This was achieved for a gain corresponding to 10 kΩ and inside a region corresponding to drive currents between 0.4 mA to 0.8 mA. This in turn corresponds to generated photocurrents between 1.29 μA to 4.16 μA. It is difficult to say why the slope of the estimate q changes and gets worse after this point but it corresponds relatively well to the sudden decrease in RMS observed in fig. 4.5 for drive currents above 1 mA. When referring to fig. 4.4, this region seems to be just at the beginning of the linear region of the photodiode response. It could be the case that increased driving current causes the noise spectrum to shift upwards and towards higher frequencies. This would then mean that more noise power is included more and more in the pass-band above 8 MHz and thus the RMS should increase. When looking at the noise spectra in figs. 4.7 to 4.9 it is however difficult to tell if this is the case for the gain corresponding to 10 kΩ.

The reason for the apparent non-linearity for 10 kΩ in fig. 4.12 compared to the more linear looking curves in fig. 4.11 is probably only due to a difference in scaling. This can be seen quite clearly when comparing the y-axis and x-axis scales of these figures.

4.4 General discussion

One of the bigger issues with this technique for generating random numbers is that it might be difficult or controversial to claim that the noise is quantum in origin. This is because it is often difficult to show that the shot noise is separated enough from the thermal noise. It can be argued though that there has to be enough shot noise present in the sampled data if the charge of the electron can be measured with quite good precision. It would not be possible to measure e if only thermal noise is present, so a large portion of the signal should contain shot noise if e is successfully estimated.

The reason that 10 kΩ appear to have the best result when estimating the electron charge could be that the noise power from the thermal noise of R_f , as described in section 2.5.1, does not yet contribute significantly to the noise at this amplification. The noise power of this thermal noise should increase as R_f increases and at some point it should also become the dominant noise source. If this is the case, this would also show that the SNR for the shot noise versus thermal noise cannot be accurately described using only eq. (2.30), which also was the expected behaviour when performing the noise analysis in section 2.5.1.

Another discussion to have is what should be required of the origin of the shot noise. According to the theory, a very inefficient photodetector (i.e. with low quantum efficiency) should exhibit shot noise. In essence, this observation should not require the existence of photons, only that the detector process behaves in a Poissonian way. If this really constitutes a true quantum source is not completely evident. If the shot noise instead really originates from the light field itself being quantized the source could probably really be considered as being quantum in origin.

The shot noise that was measured in the favourable region between 0.4 mA to 0.8 mA corresponded to measured photocurrents of 1.29 μ A to 4.16 μ A. Because this is significantly higher than the dark current (0.15 nA) of the photodiode, this is evidence for the fact that the shot noise is originating from the light field. It could thus be argued that the shot noise that was measured really was of quantum origin. It is not sure however if this is completely conclusive.

4.4.1 Discussion of method

The amplifier used in the project only consisted of one operational amplifier and is thus quite simple in construction. If more time was available it would have been interesting to compare different amplifier alternatives. Both in order to compare different op-amps but also other circuit topologies like a two step amplifier where the initial TIA is followed by a voltage amplifier.

The theoretical noise analysis (section 2.5.1) could have been more comprehensive and a more accurate value for at what amplification the thermal noise starts to dominate over noise voltage could have been calculated. This could then further prove whether $10\text{ k}\Omega$ should be optimal for this setup.

The transfer function could have been obtained not only for the electrical domain but also for the optical and electrical domains together. This way, it could be investigated how the frequency characteristics of the LED and PD affected the overall transfer function. It is not certain, however, in what way the transfer function of the LED should affect the overall bandwidth. Since it can be argued that the shot noise originates both from the light-field between the emitter and detector, but also originating in the detector itself, a severely bandwidth limited emitter would likely not affect how fast the detector could respond. The result of this experiment could thus be misleading and moreover an emitter of much faster response times than the detector would be needed in order to correctly characterize the detectors frequency response. Instruments with the capability of generating a really fast light-pulse would thus be needed and because of the complexity of this setup together with the limited resources this evaluation was not performed within the scope of the project.

The main thing that should've been tested if time allowed was to change the current source to a battery which should exhibit much less noise in the driving current. It would be interesting to see if the $1/f$ corner of the op-amp could be resolved in a system with less technical noise. If this were to be the case, the whole frequency band of region 2 could probably be utilized and it would maybe be possible to isolate the shot noise even further.

4.5 The work in a wider context

One ethical aspect to take into account when implementing these kinds of random number generators is that the security aspect is very important. It is vital that results are scrutinized and that the security really is as good as advertised. It is also important that users can trust

the research in this field for these devices to be usable by users that cannot be expected to assess the security themselves. The well known mantra "*Don't roll your own crypto*" is somewhat related to this. If you are not absolutely sure that you can develop a secure random number generator, you should probably refrain from doing so. Research must however move forward, so it is important that researchers do not become afraid or discouraged to test new ideas for generating random numbers. In the light of this I think this project constitutes a good first step and proof of concept, but further development and theoretical analysis is needed in order to construct a device that with certainty could be said to be secure.

Conclusion

This project demonstrates the expected behaviour of a simple but effective photodiode amplifier circuit that achieves high bandwidths. The stability for the lower gain configurations could however be improved upon. The presence of shot noise is demonstrated by estimating the electron charge to an accurate degree. The achieved bandwidths of the prototype could result in quite fast generation bitrates if an effective quantization scheme can be developed.

As described in the discussion in section 4.4.1 it would be valuable to see if the estimation of electron charge becomes more reliable if a current source exhibiting less noise could be used. This could be a battery when testing in the lab but in the future it should also be tested using a variable current supply located on the same board. This way the generator could control and set the driving current in order to intermittently perform self-testing by calculating estimates of e . A QRNG building on this project could utilize this estimation technique as the basis of a self-testing scheme in order to show that quantum behaviour is present. This self-testing scheme would however need further development and testing in order to be conclusive.

5.1 Future work

In essence this e estimate method is a positive test for the presence of shot noise. It would however be interesting if a negative test for the presence of thermal noise could be constructed. A possible solution could be to try to estimate k_B from the data and consider the test successful if the achieved estimate is really imprecise. This would in essence mean that the sampled noise deviated a lot from thermal noise and thus thermal noise is likely not present in the signal.

An effective, both in terms of entropy gathering and computation wise, digitization scheme together with extraction should be investigated for this kind of generator. The difficulty probably lies in how to quantize the sampled time series into some kind of variable with low correlation that then in turn would not require that much extraction when generating the random numbers.

Bibliography

- [1] J.G. Graeme. *Photodiode Amplifiers: OP AMP Solutions*. Gain technology. McGraw-Hill Education, 1996.
- [2] Miguel Herrero-Collantes and Juan Carlos Garcia-Escartin. "Quantum random number generators". en. In: *Reviews of Modern Physics* 89.1 (2017), p. 015004. DOI: 10.1103/RevModPhys.89.015004.
- [3] Sanjeev Sisodiya Landon Curt Noll Robert G. Mende. *Method for seeding a pseudo-random number generator with a cryptographic hash of a digitization of a chaotic system*. U.S. Patent US5732138A, Jan. 1996.
- [4] Bruno Sanguinetti, Anthony Martin, Hugo Zbinden, and Nicolas Gisin. "Quantum Random Number Generation on a Mobile Phone". en. In: *Physical Review X* 4.3 (2014), p. 031056. DOI: 10.1103/PhysRevX.4.031056.
- [5] Jakub Niemczuk. "Shot noise-based quantum random number generator". en. In: *Quantum Technologies 2020*. Ed. by Sara Ducci, Eleni Diamanti, Nicolas Treps, and Shannon Whitlock. SPIE, 2020, p. 44. DOI: 10.1117/12.2554898.
- [6] Mark Fox. *Quantum optics: an introduction*. Oxford master series in atomic, optical, and laser physics. Oxford: Oxford Univ. Press, 2006.
- [7] S.O. Kasap. *Optoelectronics and Photonics: Principles and Practices*. 2nd. Pearson, 2012.
- [8] Philip C. D. Hobbs. *Building Electro-Optical Systems: Making it all Work*. 3rd. 2022.
- [9] M. Reznikov, R. de Picciotto, and M. Heiblum. "Quantum shot noise". en. In: *Superlattices and Microstructures* 23.3 (1998).
- [10] Burr-Brown Corporation. *Burr-Brown IC Applications Handbook*. Pearson, 1994.
- [11] *Silicon PIN Photodiode TEFD4300*. 83471. Rev. 1.2. Vishay Semiconductors. 2014. URL: <https://www.vishay.com/docs/83471/tefd4300.pdf>.
- [12] *500MHz Ultra-Low Bias Current FET Input Op Amp*. LTC62689f. Linear Technology. 2014. URL: <https://www.analog.com/media/en/technical-documentation/data-sheets/3600fd.pdf>.
- [13] *Infrared emitting diode L-7104F3BT*. Rev. V.16A. Kingbright. 2020. URL: [https://www.kingbright.com/attachments/file/psearch/000/00/00/L-7104F3BT\(Ver.16A\).pdf](https://www.kingbright.com/attachments/file/psearch/000/00/00/L-7104F3BT(Ver.16A).pdf).
- [14] MIT Department of Physics. *Johnson Noise and Shot Noise: The Determination of the Boltzmann Constant, Absolute Zero Temperature and the Charge of the Electron*. Lab compendium for physics lab. 2013.

Images

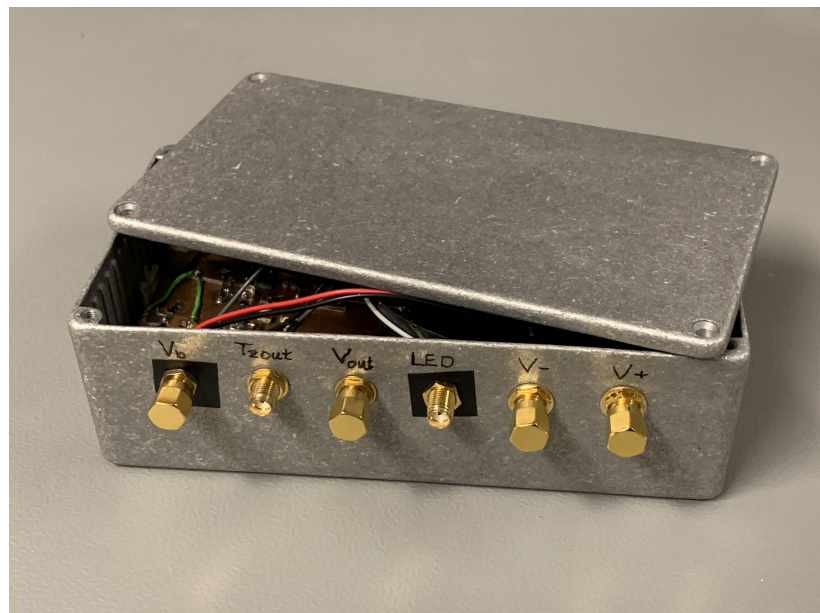


Figure A.1: The measurement box that was constructed during the project. SMA connectors can be seen on the front side to allow pass-through of cables for driving or measuring signals.

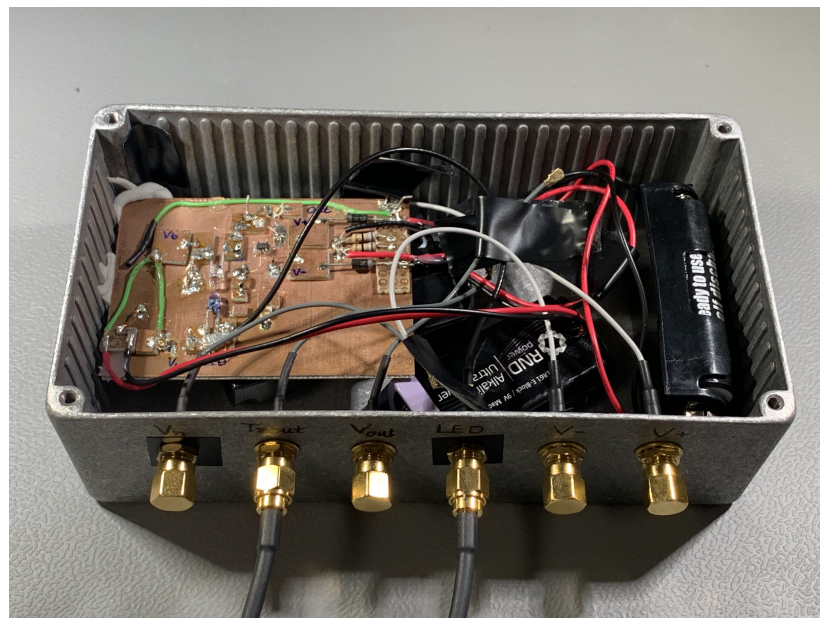


Figure A.2: The prototype equipped with batteries inside the shielding box ready for performing measurements.

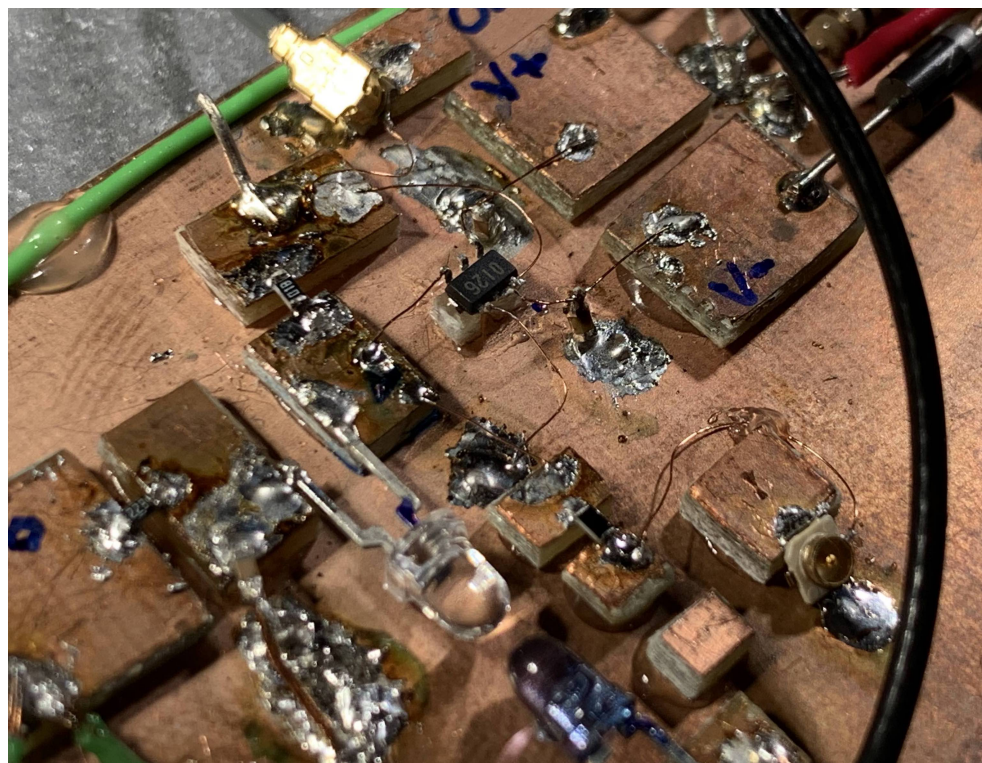


Figure A.3: The operational amplifier mounted on the prototype board "dead bug"-style (i.e. upside down).